pathway may take place constitutively in mammals (17). In cultured cells, inhibition of macroautophagy does not alter enhanced green fluorescent protein (EGFP) levels (18) or glyceraldehyde-3-phosphate dehydrogenase protein levels,[3] suggesting that not all cytosolic proteins are degraded by macroautophagy. To date, however, there have been no reports of macroautophagy in mutant SOD1 clearance.

In this study, we investigated the pathway by which human wild-type SOD1 and the A4V, G85R, and G93A SOD1 mutants are degraded in neuronal and nonneuronal cells. We show that wild-type and mutant SOD1 proteins are degraded by both the proteasomal pathway and macroautophagy. The experiments with inhibitors of these degradation pathways suggested that mutant SOD1 are degraded more rapidly than wild-type SOD1 in part by macroautophagy and that the contribution of macroautophagy to mutant SOD1 clearance is approximately equal to that of the proteasome pathway. Macroautophagy decreases mutant SOD1 protein levels in both nonionic detergent-soluble and -insoluble fractions. In addition, we provide data indicating that macroautophagy has a role in mutant SOD1-mediated cell death.

EXPERIMENTAL PROCEDURES

Plasmid Constructs—The expression plasmids pcDNA3-hSOD1 containing wild-type, A4V, G85R, and G93A mutant SOD1 were kindly donated by Ryosuke Takahashi (Kyoto University, Kyoto, Japan) and Makoto Urushitani (Laval University, Quebec, Canada) (19). To construct a plasmid expressing human wild-type SOD1 with the HA tag at the carboxyl terminus of SOD1, HA-tagged SOD1 fragments were amplified by PCR using wild-type SOD1 cDNA (Open Biosystems, Huntsville, AL) as the template. The PCR products were digested with XhoI and NotI and cloned into an XhoI-NotI-digested pCI-neo vector (Promega, Madison, WI). The primers used were 5′-AAAACTCGAGCCGCCAAGATGGCGACGAAGGCCGTGTGCG-3′ and 5′-AAAAGCGGCCGCTTAAGCGTAATCTGGAACATCGTATGGGTATTGGGCGATCCCAATTACACCACA-3′. A plasmid expressing HA-tagged G93A SOD1 was generated using QuikChange site-directed mutagenesis kit (Stratagene, La Jolla, CA) according to the manufacturer's protocol. To construct a plasmid expressing fusion protein of green fluorescent protein and LC3, LC3 fragments were amplified by PCR using rat LC3 cDNA (Open Biosystems) as the template. The PCR products were digested with BglII and EcoRI and cloned into a BglII-EcoRI-digested pEGFP-C1 vector (Clontech). The primers used were 5′-ACTCAGATCTATGCCGTCCGAGAAGACCTTCAAA-3′ and 5′-TGCAGAATTCTTACACAGCCAGTGCTGTCCCGAA-3′. After construction, the DNA sequences of the plasmids were confirmed by DNA sequence analysis.

Cell Culture and Transfection—The mouse neuroblastoma cell line Neuro2a, the human neuroblastoma cell line SH-SY5Y, and the monkey kidney-derived cell line COS-7 were maintained in Dulbecco's modified Eagle's medium (Sigma) supplemented with 10% fetal calf serum (JRH Biosciences, Lenexa, KS). Transient expression of each vector in Neuro2a and COS-7 cells was performed using the FuGENE 6 transfection reagent (Roche Applied Science). For experiments with differentiated Neuro2a cells, the medium was changed to differentiation medium (Dulbecco's modified Eagle's medium supplemented with 1% fetal calf serum and 20 μM retinoic acid) 24 h after transfection. Approximately 90% of cells in dishes (wells) were transfected in our experimental conditions (data not shown), and there was no notable differences in the transfection efficiency among the wells (supplemental Fig. S1).

Treatment of Cells with Epoxomicin, 3-Methyladenine, Cycloheximide, Rapamycin, or NH_4Cl—Cells grown in 12- or 6-well plates to 50–80% confluence were transfected with expression plasmids containing wild-type, A4V, G85R, or G93A mutant SOD1. 24 h after transfection, cells were incubated with epoxomicin (10 nM, 1 μM, 5 μM, or 10 μM; Sigma), 3-methyladenine (3-MA) (10, 20, or 30 mM; Sigma), rapamycin (100 or 200 nM; Sigma), 20 mM NH_4Cl, and/or carrier (Me_2SO or water) as a control. In some experiments, 10 μg/ml cycloheximide (Sigma) was added to the cells to avoid the confounding effects of ongoing protein synthesis. Epoxomicin, cycloheximide, and rapamycin were dissolved in Me_2SO, NH_4Cl in water. 3-MA was freshly dissolved in culture medium 30 min before use.

Cell Fractionation—For preparation of nonionic detergent-soluble and -insoluble fractions, adherent cells were harvested and lysed on ice for 15 min in 1% Triton X-100 lysis buffer containing 50 mM Tris-HCl, pH 7.5, 150 mM NaCl, 5 mM EDTA, 1% Triton X-100, and protease inhibitors (Complete, EDTA-free; Roche Applied Science). Lysates were centrifuged at 20,000 × *g* for 10 min at 4 °C, and the supernatants were pooled and designated as the detergent-soluble fractions. After the pellets were washed with 1% Triton X-100 lysis buffer, they were solubilized with SDS buffer (50 mM Tris-HCl, pH 7.5, 150 mM NaCl, 5 mM EDTA, 3% SDS, 1% Triton X-100, and protease inhibitors) and sonicated. The resulting solution was used as the detergent-insoluble fraction. For preparation of total cell lysates containing both detergent-soluble and -insoluble fractions, cells were lysed in SDS buffer and sonicated. Protein concentrations were determined with the protein assay kit (Bio-Rad) or the DC protein assay kit (Bio-Rad).

Western Blot Analysis—Western blotting was performed using standard procedures as described previously (20). The primary antibodies used were as follows: anti-SOD1 rabbit polyclonal antibody (1:4000; Stressgen Bioreagents, Victoria, Canada), anti-α-tubulin mouse monoclonal antibody (1:4000; Sigma), anti-β-actin mouse monoclonal antibody (1:5000; Sigma), anti-HA mouse monoclonal antibody (1:4000; Sigma), anti-Beclin 1 mouse monoclonal antibody (1:500; BD Transduction Laboratories, San Diego, CA), anti-Apg7/Atg7 rabbit polyclonal antibody (1:500; Rockland, Gilbertsville, PA). After overnight incubation with primary antibodies at 4 °C, each blot was probed with horseradish peroxidase-conjugated anti-rabbit IgG or anti-mouse IgG (1:20,000; Pierce). Immunoreactive signals were visualized with SuperSignal West Dura extended duration substrate (Pierce) or SuperSignal West Femto maximum sensitivity substrate (Pierce) and detected with a chemiluminescence imaging system (FluorChem; Alpha Innotech, San Leandro, CA). The signal intensity was quantified by densitometry using FluorChem software (Alpha Innotech).

Short Interfering RNA (siRNA) Preparation and Transfection—Double-stranded siRNA targeting mouse Beclin 1, mouse Atg7 and EGFP were purchased from RNAi Co., Ltd.

[3] T. Kabuta, Y. Suzuki, and K. Wada, unpublished data.

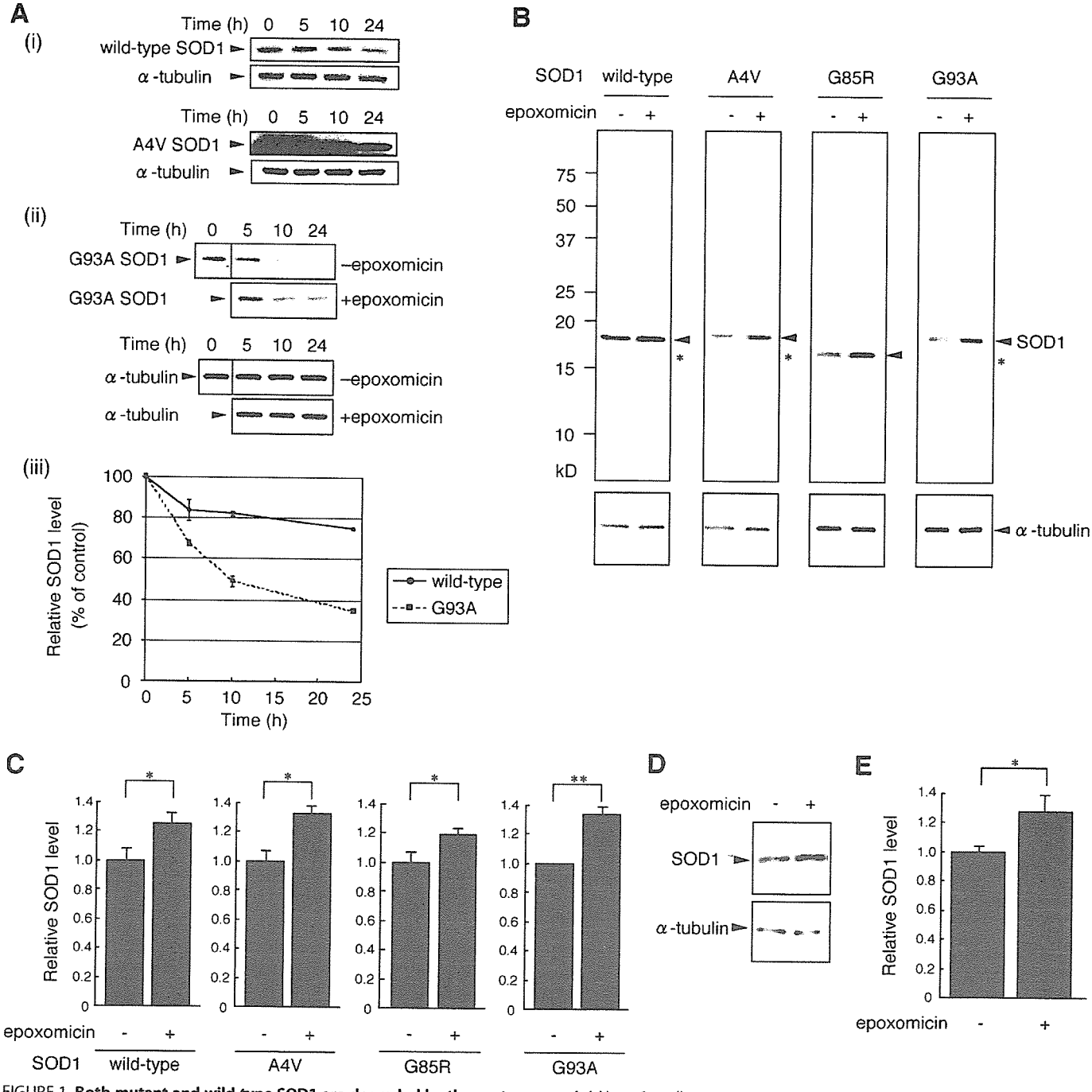

FIGURE 1. **Both mutant and wild-type SOD1 are degraded by the proteasome.** *A*, *i*, Neuro2a cells were transiently transfected with wild-type or mutant A4V human SOD1. 24 h after transfection, cells were treated with 10 μg/ml cycloheximide for the indicated time and lysed. Total cell lysates were analyzed by immunoblotting using anti-SOD1 or anti-α-tubulin antibody. *ii*, Neuro2a cells transfected with G93A SOD1 were incubated with or without 10 nM epoxomicin in the presence of 10 μg/ml cycloheximide for the indicated time and lysed. Total cell lysates were analyzed by immunoblotting using anti-SOD1 or anti-α-tubulin antibody. *iii*, the relative levels of wild-type or G93A SOD1 (percentage of 0-h control) were quantified by densitometry. Mean values are shown with S.E. ($n = 3$). *B* and *C*, Neuro2a cells were transiently transfected with wild-type or mutant A4V, G85R, or G93A human SOD1. 24 h after transfection, cells were incubated with or without 10 nM epoxomicin in the presence of 10 μg/ml cycloheximide for 24 h. Total cell lysates were analyzed by immunoblotting using anti-SOD1 antibody. The electrophoretic mobility of G85R SOD1 was greater than that of wild-type SOD1. α-Tubulin was used as a loading control. *Asterisks* indicate endogenous mouse SOD1 (*B*). The relative level of wild-type or mutant SOD1 was quantified by densitometry. Mean values are shown with S.E. ($n = 3$). *, $p < 0.05$; **, $p < 0.01$ (*C*). *D* and *E*, human SH-SY5Y cells were incubated with or without 10 nM epoxomicin in the presence of cycloheximide for 24 h. Total cell lysates were analyzed by immunoblotting with anti-SOD1 antibody (*D*). The relative level of human endogenous SOD1 was quantified by densitometry. Data are expressed as the means ± S.E. ($n = 3$). *, $p < 0.05$ (*E*).

(Tokyo, Japan). Sequences targeted by siRNA were selected using siDirect (RNAi Co., Ltd.): mouse Beclin 1 siRNA, sense (5′-GUCUACAGAAAGUGCUAAUAG-3′) and antisense (5′-AUUAGCACUUUCUGUAGACAU-3′); mouse Atg7 siRNA, sense (5′-GAGCGGCGGCUGGUAAGAACA-3′) and antisense (5′-UUCUUACCAGCCGCCGCUCAA-3′); EGFP siRNA, sense (5′-GCCACAACGUCUAUAUCAUGG-3′) and antisense (5′-AUGAUAUAGACGUUGUGGCUG-3′). EGFP siRNA was used as a control. Cells (3×10^5) were cotransfected with 1 μg of DNA and 3 μg of siRNA using Lipofectamine PLUS reagent (Invitrogen).

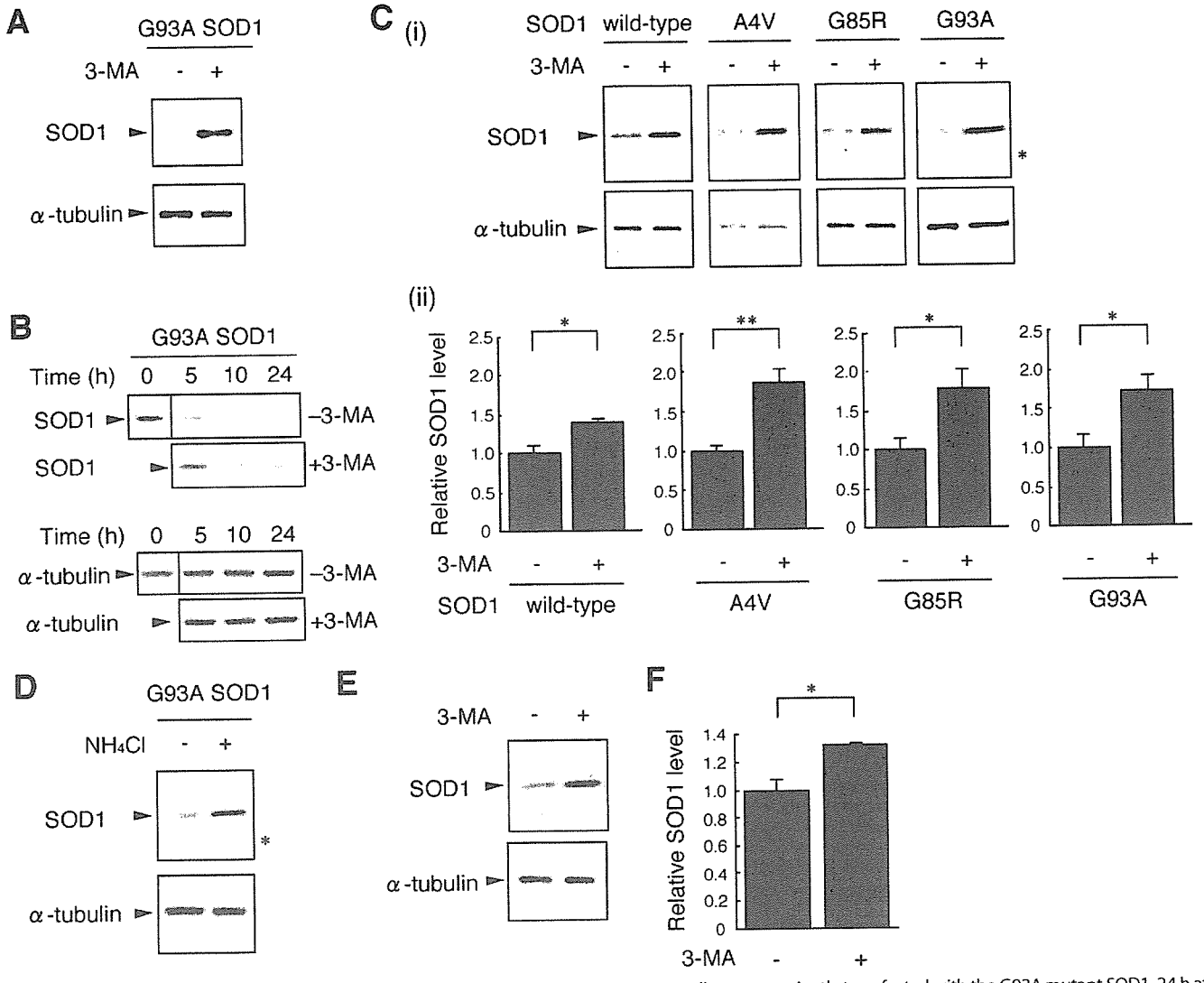

FIGURE 2. **Wild-type and mutant SOD1 are degraded by macroautophagy.** *A*, Neuro2a cells were transiently transfected with the G93A mutant SOD1. 24 h after transfection, cells were incubated with or without 10 mM 3-MA for 24 h. Total cell lysates were analyzed by immunoblotting using anti-SOD1 antibody. α-Tubulin was used as a loading control. *B*, Neuro2a cells transfected with G93A SOD1 were incubated with or without 10 mM 3-MA in the presence of 10 μg/ml cycloheximide for the indicated time and lysed. Total cell lysates were analyzed by immunoblotting using anti-SOD1 or anti-α-tubulin antibody. *C*, Neuro2a cells transfected with wild-type or mutant A4V, G85R, or G93A SOD1 were incubated with or without 10 mM 3-MA in the presence of 10 μg/ml cycloheximide for 24 h. Total cell lysates were analyzed by immunoblotting. An *asterisk* indicates endogenous mouse SOD1 (*i*). The relative level of wild-type or mutant SOD1 was quantified by densitometry. Mean values are shown with S.E. ($n = 3$). *, $p < 0.05$; **, $p < 0.01$ (*ii*). *D*, Neuro2a cells transfected with G93A SOD1 were incubated with or without 20 mM NH_4Cl in the presence of cycloheximide for 24 h. Total cell lysates were analyzed by immunoblotting. An *asterisk* indicates endogenous mouse SOD1. *E* and *F*, SH-SY5Y cells were incubated with or without 10 mM 3-MA in the presence of cycloheximide for 24 h. Total cell lysates were analyzed by immunoblotting (*E*). The relative level of human endogenous SOD1 was quantified by densitometry. Data are expressed as the means ± S.E. ($n = 3$). *, $p < 0.05$ (*F*).

Quantitative Assessment of Cell Viability and Cell Death—One day before transfection, Neuro2a cells were seeded at 5×10^4 cells/well in 24-well plates. 24 h after transfection with 0.4 μg of DNA/well, cells were cultured in differentiation medium with or without 10 mM 3-MA for 24 h. Cell death was assessed by a lactate dehydrogenase release assay using the CytoTox-ONE homogeneous membrane integrity assay (Promega) according to the manufacturer's protocol. The percentage of cytotoxicity (Fig. 7*G*) was calculated according to this protocol. For assessment of cell viability, we used the 3-(4,5-dimethylthiazol-2-yl)-5-(3-carboxymethoxyphenyl)-2-(4-sulfophenyl)-2H-tetrazolium (MTS) assay and the ATP assay with the CellTiter 96 AQueous One Solution cell proliferation assay (Promega) and CellTiter-Glo luminescent cell viability assay (Promega), respectively, according to the manufacturer's protocols. Measurements with a multiple-plate reader were performed after samples were transferred to 96-well assay plates.

Statistical Analysis—For comparison of two groups, the statistical difference was determined by Student's *t* test. For comparison of more than two groups, analysis of variance was used. If the analysis of variance was significant, Dunnett's multiple comparison test was used as a *post hoc* test.

RESULTS

Wild-type and Mutant SOD1 Are Degraded by the Proteasome—To determine whether SOD1 is degraded by the proteasome pathway, we assessed the effect of proteasome inhibitors on SOD1 protein clearance. Peptide aldehydes, such as

MG132 or ALLN, and lactacystin are widely used proteasome inhibitors. However, peptide aldehydes also inhibit cathepsins and calpains, and lactacystin inhibits cathepsin A (21, 22). Because these inhibitors are not proteasome-specific and may interfere with lysosomal function, we used epoxomicin as a selective proteasome inhibitor (23, 24). We observed protein clearance of human SOD1 in Neuro2a cells transfected with mutant or wild-type SOD1 in the presence of the translation inhibitor cycloheximide (Fig. 1*A*, *i* and *ii*). Consistent with previous reports (9, 11), wild-type SOD1 exhibited a relatively long half-life (half-life of more than 24 h) compared with mutant SOD1 (~10 h; G93A) (Fig. 1*A*, *iii*). The degradation of wild-type and mutant SOD1 was suppressed by epoxomicin treatment (Fig. 1, *B* and *C*) (~14-h increase in half-life; G93A; Fig. 1*A*, *ii*). Our finding that mutant SOD1 is degraded by the proteasome is in agreement with previous reports (8, 9). To determine whether endogenous human wild-type SOD1 is also degraded by the proteasome, SOD1 clearance was examined using the human neuroblastoma SH-SY5Y cell line. The proteasome inhibitor treatment promoted the accumulation of human SOD1 proteins (Fig. 1, *D* and *E*). These results indicate that endogenous wild-type SOD1 is degraded by the proteasome, also consistent with a previous report (14).

Wild-type and Mutant SOD1 Are Also Degraded by Macroautophagy—To date, there have been no reports of macroautophagy participating in human SOD1 clearance. We therefore investigated whether wild-type or mutant SOD1 was degraded by macroautophagy using 3-MA, an inhibitor of macroautophagy (18, 25, 26), and ammonium chloride, an inhibitor of lysosomal proteolysis (26). We initially confirmed that 3-MA inhibits the formation of autophagosomes in Neuro2a cells using green fluorescent protein-LC3, a marker of autophagosomes (27) (supplemental Fig. S2). Moreover, we also showed that the clearance of α-synuclein, an established substrate for macroautophagy (28), was inhibited by 3-MA or ammonium chloride treatment (supplemental Fig. S3). Treatment of Neuro2a cells with 3-MA promoted the accumulation of G93A mutant SOD1 proteins (Fig. 2*A*). In the presence of cycloheximide, the degradation of wild-type and mutant SOD1 was suppressed by treatment with 3-MA (Fig. 2, *B* and *C*) (a more than 14-h increase in half-life; G93A, Fig. 2*B*), indicating that wild-type and mutant SOD1 are degraded by macroautophagy in these cells and that the accumulation of SOD1 proteins by 3-MA is not due to increased protein synthesis. These results, together with Fig. 1, suggest that mutant SOD1 are degraded more rapidly than wild-type SOD1 by macroautophagy (it is estimated that 15–20% of wild-type SOD1 and 25–30% of mutant SOD1 were degraded by macroautophagy during the 24-h incubation). The clearance of mutant G93A SOD1 was also decreased by treatment with ammonium chloride (Fig. 2*D*). As shown in Supplemental Fig. S4 and Fig. 2*D*, the protein level of endogenous mouse SOD1 was increased by 3-MA or ammonium chloride treatment. The result shown in Fig. 2*D* further supports the role of the lysosomes in SOD1 degradation. To test the role of macroautophagy on SOD1 degradation in differentiated neuronal cells or neurons, we also used differentiated Neuro2a cells. In differentiated Neuro2a cells, 3-MA increased both wild-type and mutant SOD1 protein levels in the presence or absence of cycloheximide (data not shown). To determine whether endogenous human SOD1 is degraded by macroautophagy, the clearance of endogenous SOD1 was examined in SH-SY5Y cells. As shown in Fig. 2, *E* and *F*, the degradation of endogenous SOD1 proteins was inhibited by 3-MA.

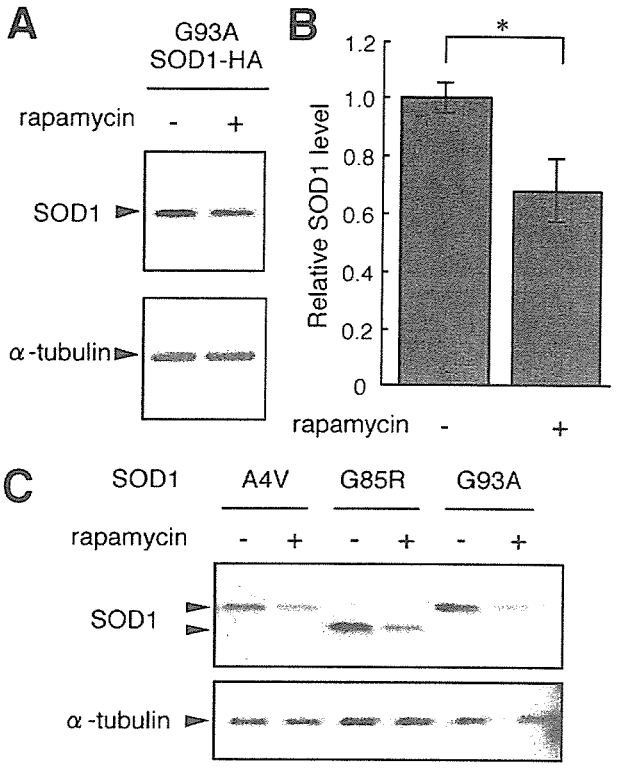

FIGURE 3. **Rapamycin treatment decreases mutant SOD1 protein levels.** *A* and *B*, Neuro2a cells were transiently transfected with HA-tagged G93A SOD1. 24 h after transfection, cells were incubated with or without 100 nM rapamycin for 24 h. Total cell lysates were analyzed by immunoblotting using anti-SOD1 antibody. α-Tubulin was used as a loading control (*A*). The relative level of mutant G93A SOD1 was quantified by densitometry. Data are presented as the means ± S.E. ($n = 3$). *, $p < 0.05$ (*B*). *C*, Neuro2a cells transfected with mutant A4V, G85R, or G93A SOD1 were cultured in differentiation medium with or without 200 nM rapamycin for 24 h. Total cell lysates were analyzed by immunoblotting.

For further confirmation of the clearance of SOD1 by macroautophagy, we used rapamycin to induce macroautophagy (29, 30), and gene silencing with siRNA to inhibit macroautophagy. Treating Neuro2a cells with rapamycin decreased HA-tagged G93A SOD1 levels (Fig. 3, *A* and *B*). In differentiated Neuro2a cells, SOD1 protein levels were also decreased by rapamycin (Fig. 3*C*). Beclin 1 is a component of a class III phosphatidylinositol 3-kinase complex that is crucial for macroautophagy (31). Silencing of the Beclin 1 gene by siRNA inhibits the generation of autophagosomes, thus preventing macroautophagy (32). Atg7 protein is also essential for macroautophagy (17). We initially confirmed that Beclin 1 or Atg7 expression was knocked down by Beclin 1 or Atg7 siRNA, respectively (Fig. 4, *A* and *B*). We also showed that α-synuclein level was increased by Beclin 1 or Atg7 siRNA (supplemental Fig. S3). We observed inhibited degradation of wild-type and mutant SOD1 in cells with Beclin 1 siRNA (Fig. 4, *A* and *C*) or Atg7 siRNA (Fig. 4, *B* and *D*) compared with cells with control siRNA (~14 h increase in half-life; G93A; Fig. 4*E*). The results shown in Figs. 2–4 demonstrate that wild-type and mutant SOD1 are also

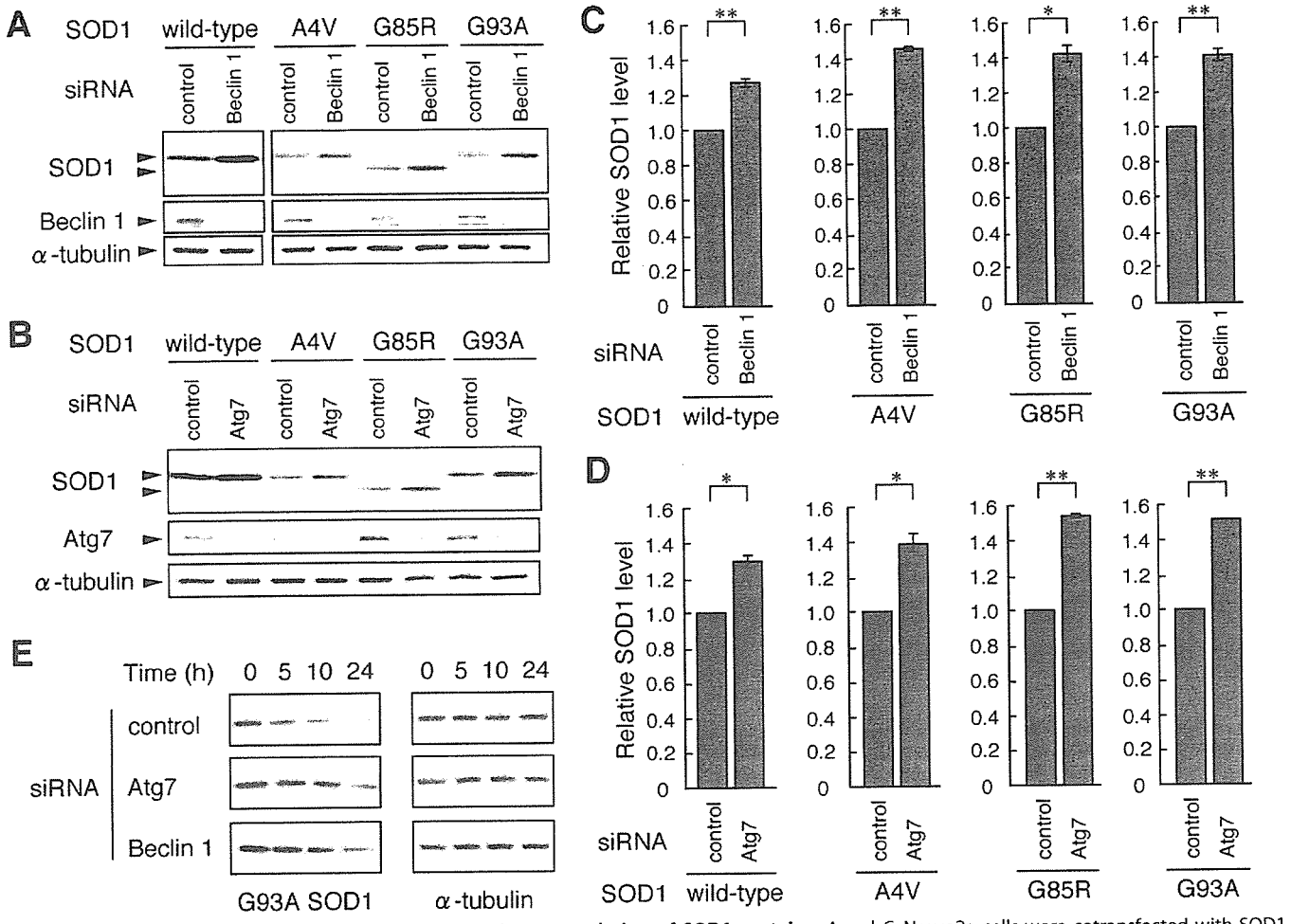

FIGURE 4. **Silencing of macroautophagy genes promote the accumulation of SOD1 proteins.** *A* and *C*, Neuro2a cells were cotransfected with SOD1 (wild-type, A4V, G85R, or G93A) and siRNA (Beclin 1 siRNA or control EGFP siRNA). 24 h after transfection, total cell lysates were prepared and analyzed by immunoblotting using anti-SOD1 or anti-Beclin 1 antibody. α-Tubulin was used as a control (*A*). Levels of SOD1 were quantified by densitometry, and the levels are expressed as -fold level of SOD1 in cells with Beclin 1 siRNA over cells with control siRNA. Data are presented as the means ± S.E. ($n = 3$). *, $p < 0.05$; **, $p < 0.01$ (*C*). *B* and *D*, Neuro2a cells were cotransfected with SOD1 (wild-type, A4V, G85R, or G93A) and siRNA (Atg7 siRNA or control siRNA). 24 h after transfection, total cell lysates were prepared and analyzed by immunoblotting using anti-SOD1, anti-Atg7, or anti-α-tubulin antibody (*B*). Levels of SOD1 were quantified by densitometry, and the levels are expressed as -fold level of SOD1 in cells with Atg7 siRNA over cells with control siRNA. Data are presented as the means ± S.E. ($n = 3$). *, $p < 0.05$; **, $p < 0.01$ (*D*). *E*, Neuro2a cells cotransfected with G93A SOD1 and siRNA (control, Atg7, or Beclin 1 siRNA) were treated with 10 μg/ml cycloheximide for the indicated time and lysed. Total cell lysates were analyzed by immunoblotting using anti-SOD1 or anti-α-tubulin antibody.

degraded by macroautophagy in neuronal cells. In the nonneuronal COS-7 cells, ammonium chloride or 3-MA treatment stimulated the accumulation of HA-tagged wild-type SOD1 and G93A SOD1 (Fig. 5*A*) or mutant G93A SOD1 (Fig. 5*B*), respectively. Treatment of the cells with epoxomicin also increased wild-type and mutant SOD1 levels (Fig. 5*C* and supplemental Fig. S5). These results indicate that wild-type and mutant SOD1 are degraded by both macroautophagy and the proteasome in COS-7 cells. The results shown in Figs. 3*A* and 5*A* indicate that not only SOD1 without a tag but also HA-tagged SOD1 is degraded by macroautophagy.

The Contributions of the Proteasome Pathway and Macroautophagy to Mutant SOD1 Degradation Are Comparable—We then assessed the relative contributions of proteasomal degradation and macroautophagy to the clearance of mutant SOD1. As shown in Fig. 6*A*, 10 mM 3-MA entirely suppresses the (3-MA-sensitive) macroautophagy-mediated degradation of mutant SOD1. 1 μM epoxomicin also entirely suppresses the (epoxomicin-sensitive) proteasome-mediated degradation of mutant SOD1 (Fig. 6*B* and supplemental Fig. S6). Therefore, we compared mutant G93A SOD1 levels in 1 μM epoxomicin-treated cells with that of 10 mM 3-MA-treated cells. The SOD1 protein level in 3-MA-treated cells was comparable with that of epoxomicin-treated cells (Fig. 6, *C–F*). An increased accumulation of mutant SOD1 was detected in cells cotreated with both inhibitors compared with that of 3-MA-treated cells or epoxomicin-treated cells (Fig. 6, *E* and *F*). These data further support the idea that mutant SOD1 proteins are degraded by both macroautophagy and the proteasome and indicate that, in these cells, the contribution of macroautophagy to mutant SOD1 clearance is approximately equal to that of the proteasome pathway.

Macroautophagy Reduces the Toxicity of Mutant SOD1—Previous studies have shown that mutant SOD1-expressing cells are more susceptible to cell death induced by proteasome inhibition (33). We examined whether inhibiting the macroautophagy-mediated degradation of mutant SOD1 could also induce cell death in Neuro2a cells using three different assays.

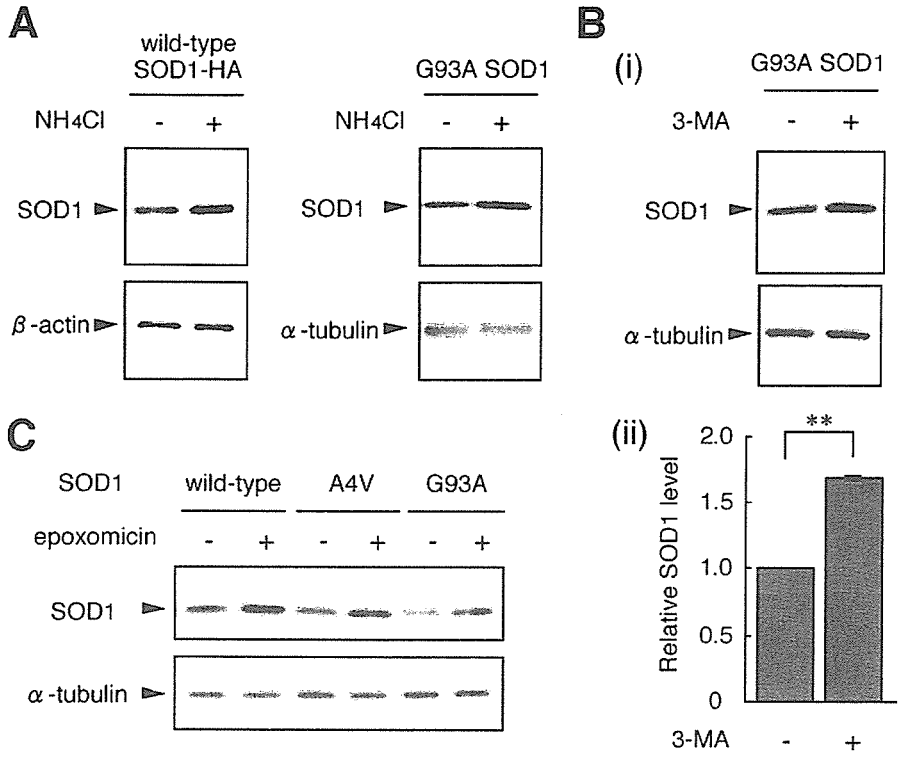

FIGURE 5. **Mutant and wild-type SOD1 are degraded by both macroautophagy and the proteasome in COS-7 cells.** *A*, COS-7 cells were transiently transfected with HA-tagged human wild-type SOD1 or G93A SOD1. 24 h after transfection, cells were incubated with or without 20 mM NH_4Cl for 24 h. Total cell lysates were analyzed by immunoblotting using anti-HA antibody or anti-SOD1 antibody. β-Actin and α-tubulin were used as loading controls. *B*, COS-7 cells transfected with G93A mutant SOD1 were incubated with or without 10 mM 3-MA in the presence of cycloheximide for 24 h. Total cell lysates were analyzed by immunoblotting using anti-SOD1 antibody (*i*). Levels of SOD1 were quantified by densitometry, and the levels are expressed as -fold level of SOD1 in cells with 3-MA over control. Data are presented as the means ± S.E. ($n = 3$). **, $p < 0.01$ (*ii*). *C*, COS-7 cells were transfected with wild-type or mutant A4V or G93A SOD1. 24 h after transfection, cells were incubated with or without 10 nM epoxomicin for 24 h. Total cell lysates were analyzed by immunoblotting.

For assessment of cell viability, we used the MTS assay and ATP assay, and for assessment of cell death, we used the lactate dehydrogenase release assay. In untreated differentiated Neuro2a cells, there was no statistically significant difference in cell viability or cell death among control cells, wild-type SOD1-expressing cells, and mutant SOD1-expressing cells (Fig. 7, *A–C*). However, when cells were treated with 3-MA, mutant SOD1-expressing cells showed significantly increased cell death and significantly decreased cell viability compared with control cells or wild-type SOD1-expressing cells (Fig. 7, *D–F*). When compared with cell death of 3-MA-untreated cells, cell death of 3-MA-treated cells was increased in mutant SOD1-expressed cells but not in cells with wild-type SOD1 (Fig. 7*G*). From these results, we conclude that macroautophagy reduces mutant SOD1-mediated toxicity in this cell model.

Inhibition of Macroautophagy Leads to Accumulation of both Detergent-soluble and Detergent-insoluble Mutant SOD1—Detergent-insoluble SOD1 proteins, aggregates, or inclusion bodies have been found in motor neurons in fALS patients (34), mouse models of fALS (35), and the cells transfected with mutant SOD1 (9, 36), although it is not clear whether these insoluble SOD1 proteins and aggregates are toxic because of conflicting results on the correlation between aggregate formation and cell death (36, 37). We investigated the effect of macroautophagy inhibition on the clearance of nonionic detergent-soluble and -insoluble SOD1. The nonionic detergent-soluble and -insoluble fractions were subjected to SDS-PAGE following Western blotting. In agreement with a previous report (9), mutant SOD1 proteins exhibited increased nonionic detergent insolubility compared with wild-type SOD1 (Fig. 8*B*). The increased level of wild-type SOD1 compared with mutant in the detergent-soluble fraction (Fig. 8*A*) is probably due to the rapid turnover of mutant SOD1. Incubation with 3-MA increased monomer SOD1 levels in the detergent-soluble (Fig. 8*A*) and -insoluble fractions (Fig. 8*B*), suggesting that both detergent-soluble and -insoluble SOD1 are degraded by macroautophagy. Consistent with a previous report (9), we found SDS-resistant dimers and high molecular weight aggregates of mutant SOD1 in the detergent-insoluble fraction (Fig. 8*C*). These dimers and aggregates of mutant SOD1 were increased by 3-MA treatment (Fig. 8*C*), suggesting that insoluble aggregates of mutant SOD1 are also cleared by macroautophagy. The results from Figs. 7 and 8 indicate that the accumulation of toxic mutant SOD1 proteins by macroautophagy inhibition leads to greater cell death.

DISCUSSION

Using inhibitors of macroautophagy and proteasomal degradation, we have shown that both wild-type and mutant SOD1 proteins are degraded by both pathways. Accumulating evidence has shown that mutant SOD1 is degraded by the ubiquitin-proteasome pathway (8, 9, 19). However, most of these studies have used lactacystin or a peptide aldehyde, both of which are not proteasome-specific inhibitors. Our data on the effect of the selective proteasome inhibitor epoxomicin also indicate that mutant SOD1 is degraded by the proteasome. Because wild-type SOD1 is not ubiquitinated by the ubiquitin ligases (10, 11), it has been proposed that wild-type SOD1 is not a substrate of the proteasome. However, a recent report has suggested that wild-type SOD1 can be degraded by the 20 S proteasome without ubiquitination (14). Moreover, we show here that epoxomicin treatment increases both overexpressed and endogenous wild-type SOD1 levels. Our data together with the previous reports support the idea that wild-type SOD1 is degraded by the 20 S proteasome in mammalian cells.

In this study, we demonstrated for the first time that macro-

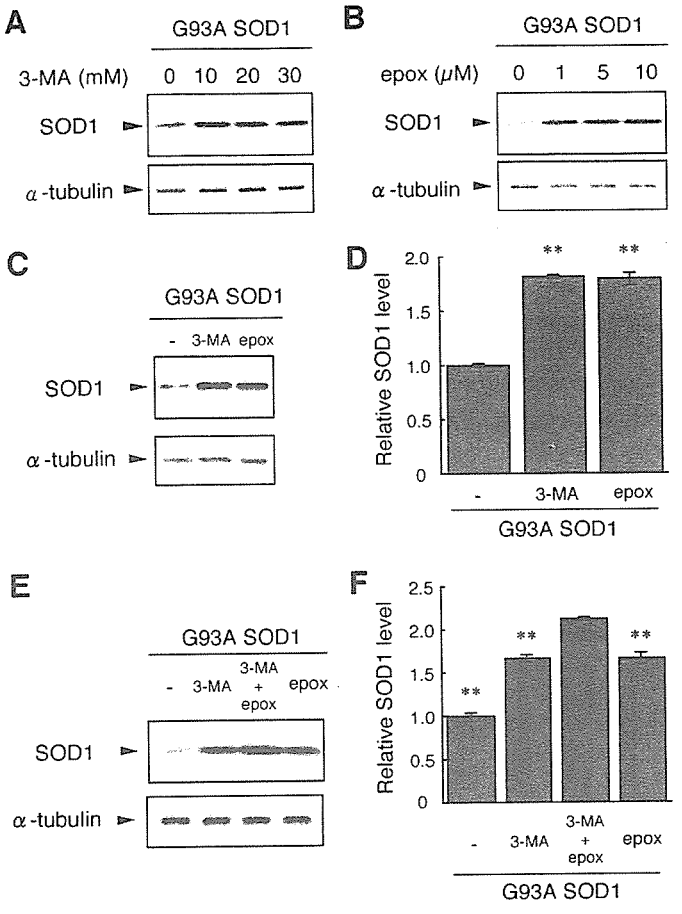

FIGURE 6. **The contribution of macroautophagy to SOD1 clearance is comparable with that of the proteasome.** *A*, Neuro2a cells transfected with mutant G93A SOD1 were incubated with or without 10, 20, or 30 mM 3-MA for 24 h. Total cell lysates were analyzed by immunoblotting. *B*, Neuro2a cells transfected with mutant G93A SOD1 were incubated with or without 1, 5, or 10 μM epoxomicin (*epox*) for 24 h. Total cell lysates were analyzed by immunoblotting. *C* and *D*, Neuro2a cells transfected with mutant G93A SOD1 were incubated with or without 10 mM 3-MA or 1 μM epoxomicin for 24 h. Total cell lysates were analyzed by immunoblotting (*C*). The relative level of mutant G93A SOD1 was quantified by densitometry. Data are presented as the means ± S.E. ($n = 3$). **, $p < 0.01$ in comparison with control (analysis of variance with Dunnett's multiple comparison test). (*D*). *E* and *F*, COS-7 cells transfected with mutant G93A SOD1 were incubated with or without 10 mM 3-MA, 1 μM epoxomicin, or both inhibitors (10 mM 3-MA and 1 μM epoxomicin) in the presence of cycloheximide for 24 h. Total cell lysates were analyzed by immunoblotting (*E*). The relative level of mutant G93A SOD1 was quantified by densitometry. Data are presented as the means ± S.E. ($n = 3$). **, $p < 0.01$ in comparison with 3-MA + epoxomicin (analysis of variance with Dunnett's multiple comparison test) (*F*).

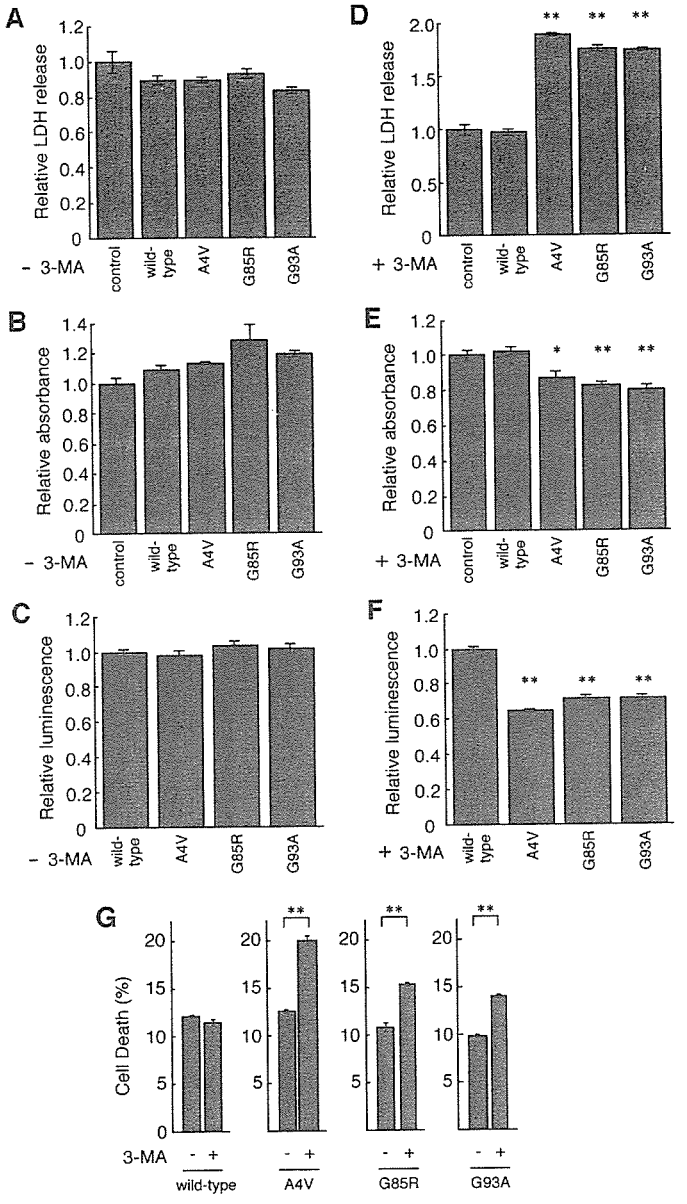

FIGURE 7. **Macroautophagy inhibition causes mutant SOD1-mediated cell death.** *A–G*, Neuro2a cells were transiently transfected with control empty vector (*A*, *B*, *D*, and *E*) or human SOD1 (wild type, A4V, G85R, or G93A). 24 h after transfection, cells were incubated in differentiation medium with (*D–G*) or without (*A–C* and *G*) 10 mM 3-MA for 24 h, and the lactate dehydrogenase release assay (*A*, *D*, and *G*), MTS assay (*B* and *E*), or ATP assay (*C* and *F*) were performed. The percentage of nonviable cells in each sample was calculated from the lactate dehydrogenase release assay (*G*). The experiment in *G* was performed independently of *A* and *D*. Data are expressed as the means ± S.E. ($n = 4$ in *A*, *C*, *D*, *F*, and *G*; $n = 3$ in *B* and *E*). *, $p < 0.05$; **, $p < 0.01$ in comparison with control (*A*, *B*, *D*, and *E*) or with wild-type SOD1 (*C* and *F*) (analysis of variance with Dunnett's multiple comparison test). **, $p < 0.01$ (*G*; *t* test).

autophagy is another pathway for degradation of wild-type and mutant SOD1. Our findings are consistent with a previous report that rat wild-type SOD1 is present in autophagosomes and lysosomes in rat hepatocytes (although they did not examine whether rat SOD1 was degraded by macroautophagy in those cells) (38). We propose that the contribution of macroautophagy to mutant SOD1 degradation is comparable with that of the proteasome pathway in the cell types we tested. Recent studies have demonstrated that transgenic mice with neuron-specific expression of mutant SOD1 do not exhibit an ALS-like phenotype (39, 40) and that neurodegeneration is delayed when motor neurons expressing mutant SOD1 are surrounded by healthy nonneuronal wild-type cells (41). In addition, Urushitani *et al.* (42) have shown that chromogranins promote secretion of mutant SOD1 from cells expressing the mutant protein, and they proposed that secreted mutant SOD1 can be toxic to neighboring cells. These studies strongly suggest that the expression of mutant SOD1 in nonneuronal cells may be involved in mutant SOD1-mediated neurotoxicity. In nonneuronal COS-7 cells, mutant SOD1 is also degraded by both the proteasome and macroautophagy (Fig. 5). Thus, not only the proteasome but also macroautophagy may play an important

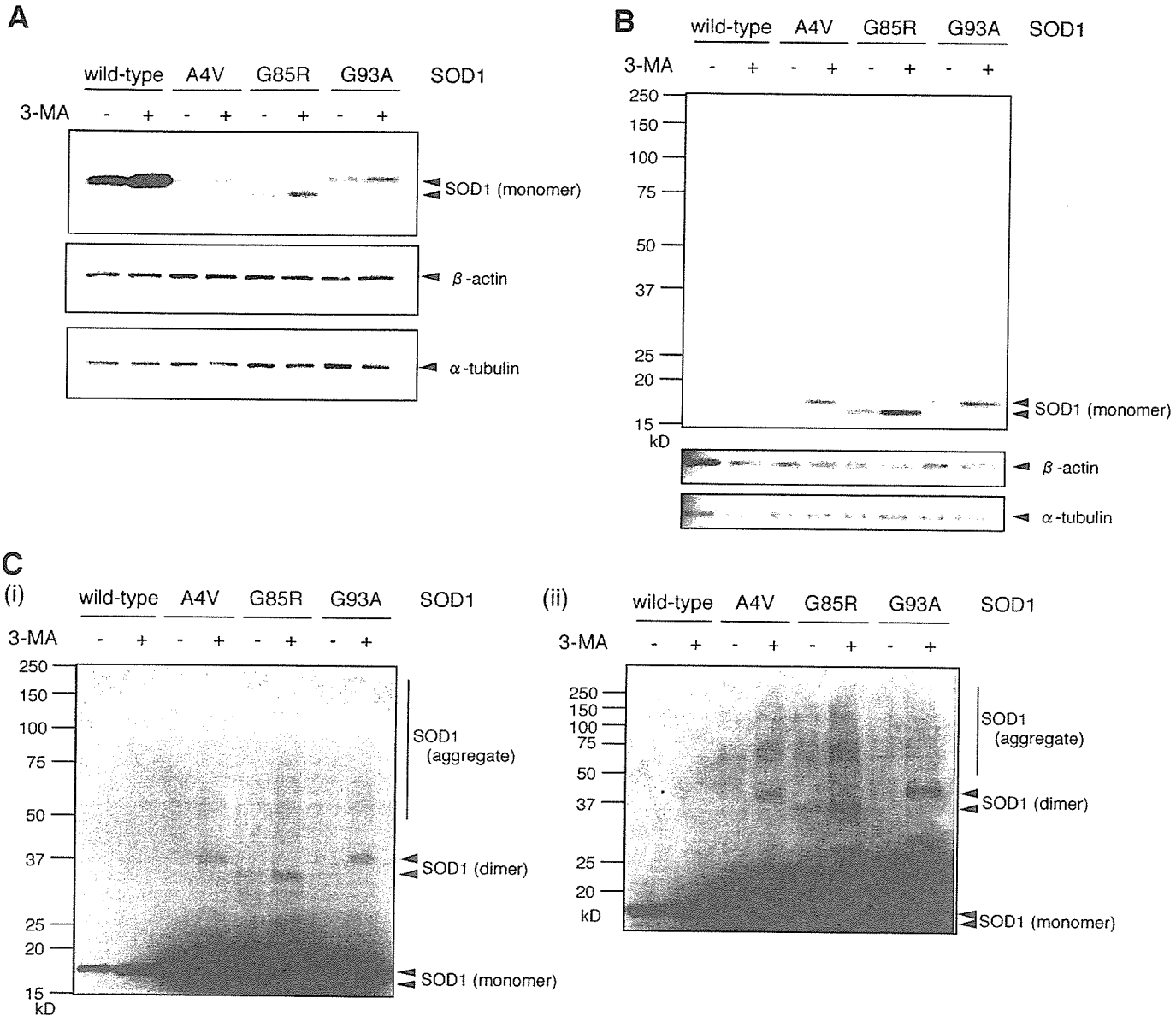

FIGURE 8. **Inhibition of macroautophagy causes accumulation of both detergent-soluble and -insoluble mutant SOD1.** *A–C*, Neuro2a cells were transiently transfected with human wild-type or mutant A4V, G85R, or G93A SOD1. 24 h after transfection, cells were cultured in differentiation medium with or without 10 mM 3-MA for 24 h. Triton X-100-soluble (*A*) and -insoluble (*B* and *C*) fractions were prepared and analyzed by immunoblotting using anti-SOD1 antibody. β-Actin and α-tubulin were used as loading controls. *C* (*i*), a longer exposure of *B*. *C* (*i* and *ii*), two different sets of experiments with longer exposure.

role in clearance of mutant SOD1 in fALS in nonneuronal cells as well as in neuronal cells.

It has been well established that mutant SOD1-mediated toxicity is caused by a gain of toxic function rather than the loss of SOD1 activity (1, 2). The appearance of mutant SOD1 aggregates in motor neurons in fALS patients and mouse models of fALS (34, 35) has suggested that aggregation has a role in neurotoxicity. However, conflicting results have been reported on the correlation between aggregate formation and cell death. A recent study has shown that the ability of mutant G85R and G93A SOD1 proteins to form aggregates correlates with neuronal cell death using live cell imaging techniques (36). Another report has concluded that aggregate formation of A4V and V148G SOD1 mutants does not correlate with cell death (37). These controversies also exist in other neurodegenerative diseases (43–46). Our current data suggest that macroautophagy degrades toxic species of mutant SOD1 and that the accumulation of mutant SOD1 proteins leads to greater cell death. However, whether the toxic SOD1 species are monomers, oligomers, or aggregates cannot be determined from our study, because a variety of mutant SOD1 species, including detergent-soluble SOD1 monomers and detergent-insoluble monomers, dimers, and aggregates, were accumulated by macroautophagy inhibition (Fig. 8).

Our data show that macroautophagy reduces mutant SOD1-mediated toxicity and that induction of macroautophagy decreases mutant SOD1 protein levels. Niwa *et al.* (10) have shown that the ubiquitin ligase Dorfin ubiquitinates mutant SOD1 and prevents the neurotoxicity of mutant SOD1. Taken together, these data imply that macroautophagy inducers, acti-

vators of the ubiquitin-proteasome pathway, or a combination of the two have therapeutic potential for fALS. In conclusion, our results demonstrate that mutant SOD1 is degraded by at least two pathways, macroautophagy and the proteasome pathway, and that the clearance of mutant SOD1 by macroautophagy reduces its cell toxicity. These findings may provide insight into the molecular mechanisms of the pathogenesis of fALS.

Acknowledgments—We thank Dr. Ryosuke Takahashi (Kyoto University) and Dr. Makoto Urushitani (Laval University) for the gift of pcDNA3-hSOD1 (wild-type and mutant A4V, G85R, and G93A) plasmids, and Naoki Takagaki for the support in English.

REFERENCES

1. Bruijn, L. I., Miller, T. M., and Cleveland, D. W. (2004) *Annu. Rev. Neurosci.* **27,** 723–749
2. Cleveland, D. W., and Rothstein, J. D. (2001) *Nat. Rev. Neurosci.* **2,** 806–819
3. Rosen, D. R., Siddique, T., Patterson, D., Figlewicz, D. A., Sapp, P., Hentati, A., Donaldson, D., Goto, J., O'Regan, J. P., Deng, H. X., Rahmani, Z., Krizus, A., McKenna-Yasek, D., Cayabyab, A., Gaston, S. M., Berger, R., Tanzi, R. E., Halperin, J. J., Herzfeldt, B., Van den Bergh, R., Hung, W. Y., Bird, T., Deng, G., Mulder, D. W., Smyth, C., Laing, N. G., Soriano, E., Pericak-Vance, M. A., Haines, J., Rouleau, G. A., Gusella, J. S., Horvitz, H. R., and Brown, R. H., Jr. (1993) *Nature* **362,** 59–62
4. Gurney, M. E., Pu, H., Chiu, A. Y., Dal Canto, M. C., Polchow, C. Y., Alexander, D. D., Caliendo, J., Hentati, A., Kwon, Y. W., Deng, H. X., Chen, W., Zhai, P., Sufit, R. L., and Siddique, T. (1994) *Science* **264,** 1772–1775
5. Reaume, A. G., Elliott, J. L., Hoffman, E. K., Kowall, N. W., Ferrante, R. J., Siwek, D. F., Wilcox, H. M., Flood, D. G., Beal, M. F., Brown, R. H., Jr., Scott, R. W., and Snider, W. D. (1996) *Nat. Genet.* **13,** 43–47
6. Goldberg, A. L. (2003) *Nature* **426,** 895–899
7. Cuervo, A. M. (2004) *Trends Cell Biol.* **14,** 70–77
8. Hoffman, E. K., Wilcox, H. M., Scott, R. W., and Siman, R. (1996) *J. Neurol. Sci.* **139,** 15–20
9. Johnston, J. A., Dalton, M. J., Gurney, M. E., and Kopito, R. R. (2000) *Proc. Natl. Acad. Sci. U. S. A.* **97,** 12571–12576
10. Niwa, J., Ishigaki, S., Hishikawa, N., Yamamoto, M., Doyu, M., Murata, S., Tanaka, K., Taniguchi, N., and Sobue, G. (2002) *J. Biol. Chem.* **277,** 36793–36798
11. Miyazaki, K., Fujita, T., Ozaki, T., Kato, C., Kurose, Y., Sakamoto, M., Kato, S., Goto, T., Itoyama, Y., Aoki, M., and Nakagawara, A. (2004) *J. Biol. Chem.* **279,** 11327–11335
12. Shringarpure, R., Grune, T., Mehlhase, J., and Davies, K. J. (2003) *J. Biol. Chem.* **278,** 311–318
13. Asher, G., Tsvetkov, P., Kahana, C., and Shaul, Y. (2005) *Genes Dev.* **19,** 316–321
14. Di Noto, L., Whitson, L. J., Cao, X., Hart, P. J., and Levine, R. L. (2005) *J. Biol. Chem.* **280,** 39907–39913
15. Komatsu, M., Waguri, S., Chiba, T., Murata, S., Iwata, J., Tanida, I., Ueno, T., Koike, M., Uchiyama, Y., Kominami, E., and Tanaka, K. (2006) *Nature* **441,** 880–884
16. Hara, T., Nakamura, K., Matsui, M., Yamamoto, A., Nakahara, Y., Suzuki-Migishima, R., Yokoyama, M., Mishima, K., Saito, I., Okano, H., and Mizushima, N. (2006) *Nature* **441,** 885–889
17. Komatsu, M., Waguri, S., Ueno, T., Iwata, J., Murata, S., Tanida, I., Ezaki, J., Mizushima, N., Ohsumi, Y., Uchiyama, Y., Kominami, E., Tanaka, K., and Chiba, T. (2005) *J. Cell Biol.* **169,** 425–434
18. Ravikumar, B., Duden, R., and Rubinsztein, D. C. (2002) *Hum. Mol. Genet.* **11,** 1107–1117
19. Urushitani, M., Kurisu, J., Tsukita, K., and Takahashi, R. (2002) *J. Neurochem.* **83,** 1030–1042
20. Kabuta, T., Hakuno, F., Asano, T., and Takahashi, S. (2002) *J. Biol. Chem.* **277,** 6846–6851
21. Lee, D. H., and Goldberg, A. L. (1998) *Trends Cell Biol.* **8,** 397–403
22. Ostrowska, H., Wojcik, C., Wilk, S., Omura, S., Kozlowski, L., Stoklosa, T., Worowski, K., and Radziwon, P. (2000) *Int. J. Biochem. Cell Biol.* **32,** 747–757
23. Meng, L., Mohan, R., Kwok, B. H., Elofsson, M., Sin, N., and Crews, C. M. (1999) *Proc. Natl. Acad. Sci. U. S. A.* **96,** 10403–10408
24. Garcia-Echeverria, C. (2002) *Mini Rev. Med. Chem.* **2,** 247–259
25. Qin, Z. H., Wang, Y., Kegel, K. B., Kazantsev, A., Apostol, B. L., Thompson, L. M., Yoder, J., Aronin, N., and DiFiglia, M. (2003) *Hum. Mol. Genet.* **12,** 3231–3244
26. Cuervo, A. M., Stefanis, L., Fredenburg, R., Lansbury, P. T., and Sulzer, D. (2004) *Science* **305,** 1292–1295
27. Kabeya, Y., Mizushima, N., Ueno, T., Yamamoto, A., Kirisako, T., Noda, T., Kominami, E., Ohsumi, Y., and Yoshimori, T. (2000) *EMBO J.* **19,** 5720–5728
28. Webb, J. L., Ravikumar, B., Atkins, J., Skepper, J. N., and Rubinsztein, D. C. (2003) *J. Biol. Chem.* **278,** 25009–25013
29. Blommaart, E. F., Luiken, J. J., Blommaart, P. J., van Woerkom, G. M., and Meijer, A. J. (1995) *J. Biol. Chem.* **270,** 2320–2326
30. Gutierrez, M. G., Master, S. S., Singh, S. B., Taylor, G. A., Colombo, M. I., and Deretic, V. (2004) *Cell* **119,** 753–766
31. Liang, X. H., Jackson, S., Seaman, M., Brown, K., Kempkes, B., Hibshoosh, H., and Levine, B. (1999) *Nature* **402,** 672–676
32. Shimizu, S., Kanaseki, T., Mizushima, N., Mizuta, T., Arakawa-Kobayashi, S., Thompson, C. B., and Tsujimoto, Y. (2004) *Nat. Cell Biol.* **6,** 1221–1228
33. Aquilano, K., Rotilio, G., and Ciriolo, M. R. (2003) *J. Neurochem.* **85,** 1324–1335
34. Kato, S., Takikawa, M., Nakashima, K., Hirano, A., Cleveland, D. W., Kusaka, H., Shibata, N., Kato, M., Nakano, I., and Ohama, E. (2000) *Amyotroph. Lateral Scler. Other Motor Neuron Disord.* **1,** 163–184
35. Bruijn, L. I., Becher, M. W., Lee, M. K., Anderson, K. L., Jenkins, N. A., Copeland, N. G., Sisodia, S. S., Rothstein, J. D., Borchelt, D. R., Price, D. L., and Cleveland, D. W. (1997) *Neuron* **18,** 327–338
36. Matsumoto, G., Stojanovic, A., Holmberg, C. I., Kim, S., and Morimoto, R. I. (2005) *J. Cell Biol.* **171,** 75–85
37. Lee, J. P., Gerin, C., Bindokas, V. P., Miller, R., Ghadge, G., and Roos, R. P. (2002) *J. Neurochem.* **82,** 1229–1238
38. Rabouille, C., Strous, G. J., Crapo, J. D., Geuze, H. J., and Slot, J. W. (1993) *J. Cell Biol.* **120,** 897–908
39. Pramatarova, A., Laganiere, J., Roussel, J., Brisebois, K., and Rouleau, G. A. (2001) *J. Neurosci.* **21,** 3369–3374
40. Lino, M. M., Schneider, C., and Caroni, P. (2002) *J. Neurosci.* **22,** 4825–4832
41. Clement, A. M., Nguyen, M. D., Roberts, E. A., Garcia, M. L., Boillee, S., Rule, M., McMahon, A. P., Doucette, W., Siwek, D., Ferrante, R. J., Brown, R. H., Jr., Julien, J. P., Goldstein, L. S., and Cleveland, D. W. (2003) *Science* **302,** 113–117
42. Urushitani, M., Sik, A., Sakurai, T., Nukina, N., Takahashi, R., and Julien, J. P. (2006) *Nat. Neurosci.* **9,** 108–118
43. Arrasate, M., Mitra, S., Schweitzer, E. S., Segal, M. R., and Finkbeiner, S. (2004) *Nature* **431,** 805–810
44. Saudou, F., Finkbeiner, S., Devys, D., and Greenberg, M. E. (1998) *Cell* **95,** 55–66
45. Schaffar, G., Breuer, P., Boteva, R., Behrends, C., Tzvetkov, N., Strippel, N., Sakahira, H., Siegers, K., Hayer-Hartl, M., and Hartl, F. U. (2004) *Mol. Cell.* **15,** 95–105
46. Nucifora, F. C., Jr., Sasaki, M., Peters, M. F., Huang, H., Cooper, J. K., Yamada, M., Takahashi, H., Tsuji, S., Troncoso, J., Dawson, V. L., Dawson, T. M., and Ross, C. A. (2001) *Science* **291,** 2423–2428

Available online at www.sciencedirect.com

ScienceDirect

Neurochemistry International 50 (2007) 119–129

NEUROCHEMISTRY International

www.elsevier.com/locate/neuint

Dopaminergic neuronal loss in transgenic mice expressing the Parkinson's disease-associated UCH-L1 I93M mutant

Rieko Setsuie [a,b,1], Yu-Lai Wang [a,1], Hideki Mochizuki [c,d], Hitoshi Osaka [a,e], Hideki Hayakawa [c], Nobutsune Ichihara [f], Hang Li [a], Akiko Furuta [a], Yae Sano [a,b], Ying-Jie Sun [a], Jungkee Kwon [a,g], Tomohiro Kabuta [a], Kenji Yoshimi [d], Shunsuke Aoki [a], Yoshikuni Mizuno [c,d], Mami Noda [b], Keiji Wada [a,*]

[a] *Department of Degenerative Neurological Diseases, National Institute of Neuroscience, National Center of Neurology and Psychiatory, Kodaira, Tokyo 187-8502, Japan*

[b] *Laboratory of Pathophysiology, Graduate School of Pharmaceutical Sciences, Kyushu University, Higashi-ku, Fukuoka 812-8582, Japan*

[c] *Department of Neurology, Juntendo University School of Medicine, Bunkyo-ku, Tokyo 113-8421, Japan*

[d] *Research Institute for Diseases of Old Age, Juntendo University School of Medicine, Bunkyo-ku, Tokyo 113-8421, Japan*

[e] *Division of Neurology, Clinical Research Institute, Kanagawa Children's Medical Center, Yokohama 232-8555, Japan*

[f] *Department of Anatomy, School of Veterinary Medicine, Azabu University, Sagamihara 229-8501, Japan*

[g] *College of Veterinary Medicine, Chonbuk National University, 644-14 Duckjin-Ku, Jeonju 561-756, Republic of Korea*

Received 14 March 2006; received in revised form 19 June 2006; accepted 11 July 2006
Available online 11 September 2006

Abstract

The I93M mutation in ubiquitin carboxyl-terminal hydrolase L1 (UCH-L1) was reported in one German family with autosomal dominant Parkinson's disease (PD). The causative role of the mutation has, however, been questioned. We generated transgenic (Tg) mice carrying human *UCHL1* under control of the *PDGF-B* promoter; two independent lines were generated with the I93M mutation (a high- and low-expressing line) and one line with wild-type human UCH-L1. We found a significant reduction in the dopaminergic neurons in the substantia nigra and the dopamine content in the striatum in the high-expressing I93M Tg mice as compared with non-Tg mice at 20 weeks of age. Although these changes were absent in the low-expressing I93M Tg mice, 1-methyl-4-phenyl-1,2,3,6-tetrahydropyridine (MPTP) treatment profoundly reduced dopaminergic neurons in this line as compared with wild-type Tg or non-Tg mice. Abnormal neuropathologies were also observed, such as silver staining-positive argyrophilic grains in the perikarya of degenerating dopaminergic neurons, in I93M Tg mice. The midbrains of I93M Tg mice contained increased amounts of insoluble UCH-L1 as compared with those of non-Tg mice, perhaps resulting in a toxic gain of function. Collectively, our data represent *in vivo* evidence that expression of $UCHL1^{I93M}$ leads to the degeneration of dopaminergic neurons.

Keywords: Ubiquitin carboxy-terminal hydrolase L1; Animal model; Parkinson's disease; Dopaminergic neuron

1. Introduction

Parkinson's disease (PD) is the second most common human neurodegenerative disorder after Alzheimer's disease (AD) (Dauer and Przedborski, 2003; Vila and Przedborski, 2004). PD patients exhibit motor dysfunction, including slowed movement (bradykinesia), resting tremor, rigidity, and postural instability (Dauer and Przedborski, 2003). The pathological basis of PD is the progressive loss of dopaminergic neurons in the substantia nigra pars compacta, giving rise to a decrease in dopamine content in the striatum (Dauer and Przedborski, 2003). Although most cases of PD are sporadic, studies of familial PD have provided accumulating evidence for the molecular mechanisms of PD. Thus far, at least six proteins have been identified to cause familial PD: α-synuclein (Chartier-Harlin et al., 2004; Farrer et al., 2004; Ibanez et al., 2004; Kruger et al., 1998; Polymeropoulos et al., 1997; Singleton et al., 2003), UCH-L1 (Leroy et al., 1998), parkin (Kitada et al., 1998), DJ-1 (Bonifati et al., 2003), phosphatase

* Corresponding author. Tel.: +81 42 346 1715; fax: +81 42 346 1745.
E-mail address: wada@ncnp.go.jp (K. Wada).
[1] These authors contributed equally to this work.

0197-0186/$ – see front matter
doi:10.1016/j.neuint.2006.07.015

and tensin homolog induced kinase-1 (PINK1) (Valente et al., 2004), and leucine-rich repeat kinase-2 (LRRK2) (Paisan-Ruiz et al., 2004; Zimprich et al., 2004). α-Synuclein, UCH-L1 and LRRK2 are linked to the autosomal dominant form of PD, whereas parkin, DJ-1 and PINK1 are linked to the recessive form.

In 1998, UCH-L1 carrying an Ile to Met mutation at amino acid position 93 (I93M) was identified in one German family affected by autosomal dominant familial PD. UCH-L1, also known as PGP9.5, is an abundant protein in neuronal cells, comprising up to about 1–2% of total protein in the brain. Its function as de-ubiquitylating enzyme (Larsen et al., 1998; Wilkinson et al., 1989), ubiquitylating enzyme (Liu et al., 2002), de-neddylating enzyme (Hemelaar et al., 2004), and mono-ubiquitin stabilizer (Osaka et al., 2003) has been reported. *In vitro* analysis using recombinant human UCH-L1 indicated that I93M mutation results in the reduction of hydrolase activity of about 50% (Nishikawa et al., 2003). *Uchl1* gene deletion in mice, however, was reported to causes gracile axonal dystrophy (*gad*), a recessive neurodegenerative disease with distinct phenotype and pathological features from PD (Saigoh et al., 1999). Moreover, extensive analysis failed to find other PD patients with mutations in the *UCHL1* gene (Lincoln et al., 1999; Maraganore et al., 1999) and there was an incomplete penetrance in reported German family (Leroy et al., 1998). Thus, the correlation of I93M mutation and pathogenesis of PD was questioned.

To elucidate the pathological role of UCH-L1^{I93M} expression in the pathogenesis of PD, *in vivo*, we generated transgenic mice expressing human UCH-L1^{I93M}.

2. Experimental procedures

2.1. Generation of *hUCHL1*^{WT} and *hUCHL1*^{I93M} transgenic mice

We generated transgenes by cloning either the wild-type or I93M mutant human UCH-L1 cDNAs under the control of the human platelet-derived growth factor B chain (*PDGF-B*) promoter (Fig. 1A) (Sasahara et al., 1991). Sequences encoding *UCHL1* were amplified from a human brain cDNA library (Stratagene, La Jolla, CA) by PCR and subcloned into the *Xho*I and *Not*I sites of pCI-neo (Promega, Madison, WI). The I93M substitution was obtained using QuikChange (Stratagene). The 5′ flanking region of the human *PDGF-B* chain gene was isolated from the human genomic DNA and inserted into the *Bgl*II and *Xho*I site of pCI-neo which results in the replacement of promoter from CMV to *PDGF-B*. The plasmid was linearized by digestion with *Hin*dIII and *Aat*II. A 2 μg/ml solution of the linearized plasmid of each transgene was then microinjected into the pronuclei of newly fertilized C57BL/6J mouse eggs. Offspring were screened for the presence of the transgene by PCR of tail DNA using specific primers (forward: PD-UCH-2, 5′-GCACTCTCCCTTCTCCTTTATA-3′; reverse: PD-UCH-5, 5′-CCTGTATGGCCTCATTCTTTTC-3′). Expression of hUCH-L1^{I93M} in a low-expressing mouse line only occurred in male mice. Thus, all experiments were done using male heterozygous transgenic mice. Animal care and handling were in accordance with institutional regulations for animal care and were approved by the Animal Investigation Committee of the National Institute of Neuroscience, National Center of Neurology and Psychiatry, Tokyo, Japan which conforms the National Institute of Health guide for the care and use of Laboratory animals.

2.2. Quantitative RT-PCR analysis

Primers specific for mouse *Uchl1* (forward: mL1-7, 5′-CCTTGGTTTGCAGCTTTAGCA-3′; reverse: mL1-8, 5′-GGGCTGTAGAACGCAAGAAGA-3′) and human *UCHL1* (forward: L1Tg-F2, 5′-TGGCAACTTCTCCTCCTGCA-3′; reverse: L1Tg-R2, 5′-ACAGCACTTTGTTCAGCATC-3′) were designed, and SYBR Green-based real-time quantitative RT-PCR was performed using the ABI PRISM 7700 (Applied Biosystems, Foster City, CA) using total RNA from mouse brain ($n = 3$ for each line) (Aoki et al., 2002). GAPDH was used as an internal control.

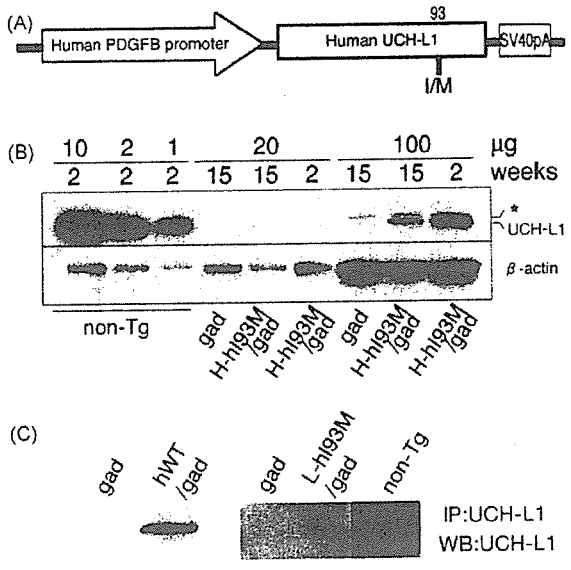

Fig. 1. Generation of transgenic mice expressing hUCH-L1^{WT} and hUCH-L1^{I93M}. (A) UCH-L1^{I93M} was constructed under control of the *PDGF-B* promoter, as depicted. (B) Immunoblotting analysis of endogenous mouse UCH-L1 and transgenic human UCH-L1 expression in mouse midbrain. To detect exogenous human UCH-L1 levels specifically, we generated transgenic mice in the *gad* background (H-hI93M/*gad*), which corresponds to the null mutant of *Uchl1*. Notice that the faint band corresponding to UCH-L1 is detected at 2 weeks of age when 20 μg protein/lane was loaded for the detergent-soluble fraction of midbrain origin in H-hI93M/*gad* mice. When the applied protein was increased to 100 μg/lane, UCH-L1 was easily detected at 2 weeks in H-hI93M/*gad* mice, and UCH-L1 levels markedly decreased by age 15 weeks. Faint bands indicated by the asterisk may correspond to UCH-L3, which cross-reacted with the UCH-L1 antibody when a large amount of protein was loaded per lane. (C) Immunoprecipitation analysis of exogenous human UCH-L1 in hWT/gad (left) and L-hI93M/gad (right) brains. Brain lysates from hWT/gad (left) or L-hI93M/gad (right) were both immunoprecipitated and detected using anti-UCH-L1 antibody. The band corresponding to the UCH-L1 can be found in both hWT/gad and L-hI93M/gad lysates but not in gad lysates indicating the exogenous human UCH-L1 expression.

2.3. Fractionation and immunoblotting and immunoprecipitation

For the immunoblotting of total UCH-L1, the soluble fraction in RIPA (20 mM Tris–HCl, pH 7.5; 0.1% SDS; 1.0% (w/v) Triton X-100; 1.0% sodium deoxycholate) with Complete EDTA-Free Protease Inhibitors (Roche, Basel, Switzerland) was extracted from H-hI93M/*gad* ([high-expressing] *UCH-L1*$^{I93M/-}$, *Uchl1*$^{gad/gad}$), *gad* and non-Tg mouse midbrains. The extracted samples were loaded as indicated in Fig. 1.

For subfractionation, the cortex and hippocampus were removed from the midbrains of a H-hI93M mouse or a non-Tg littermate and bottom half under the aqueduct were used as the substantia nigra fraction. The fractionation method was modified from that of Kahle et al. (2001). Each sample was homogenized with 9 volumes of 5% SDS/TBS lysis buffer (50 mM Tris–HCl (pH 7.5), 150 mM NaCl, 5% SDS) with Complete EDTA-Free Protease Inhibitors using a 23G syringe. After three times of 10 s sonication, samples were ultra-centrifuged in 130,000 × *g* for 1 h, and the supernatant were pooled as 5% SDS fraction. The pellets were washed with 5% SDS/TBS solution once and further homogenized in 8 M urea/5% SDS/TBS lysis buffer

(8 M urea, 5% SDS, 50 mM Tris–HCl (pH 7.5), 150 mM NaCl) with 23G syringe. The resulting supernatant was used as 8 M urea/5% SDS fraction. The protein concentration was assessed by a DC-protein assay kit (Bio-Rad). 1.25 μg of 5% SDS fraction and 0.5 μg of 8 M urea/5% SDS fraction were subjected to SDS-PAGE using 15% gels (Perfect NT Gel; DRC, Tokyo, Japan). Anti-UCH-L1 (1:5000, RA95101; Ultraclone, Isle of Wight, UK) and anti-β-actin (1:5000, clone AC15; Sigma, St. Louis, MO) were used to detect each protein. Signals were detected using a chemiluminescent SuperSignal West Dura Extended Duration Substrate kit or West Femto Maximum Sensitivity Substrate kit (Pierce, Rochford, IL) and analyzed with a ChemiImager (Alpha Innotech, San Leandro, CA). For the internal control of 8 M urea/5% SDS fraction, 1 μg protein were dot blotted to PVDF membrane and stained with Ponceau S staining (Rane et al., 2004). Statistical analyses were conducted using the two-tailed Student's *t*-test with total of four samples for each group.

For the immunoprecipitation, half of the brain (for hWT/gad) or midbrain region (for L-hI93M/gad) were homogenized in 2 ml ice-cold modified RIPA buffer (50 mM Tris–HCl, pH 7.4; 1% (w/v) Nonidet P40; 0.25% sodium deoxycholate; 150 mM NaCl; 1 mM EDTA) with Complete EDTA-Free Protease Inhibitors and centrifuged at 16,000 × *g* at 4 °C for 20 min. The protein concentration of the resulting supernatants was determined with the Protein Assay Kit (Bio-Rad, Hercules, CA). Immunoprecipitation was performed with a Seize X Mammalian Immunoprecipitation kit (Pierce, Rockford, IL) with some modifications. Briefly, 300 μg of protein was added to a 50 μl slurry of immobilized protein G cross-linked with rabbit polyclonal anti-human UCH-L1 (AB1716; Chemicon, Temecula, CA) or normal rabbit IgG and rotated at 4 °C overnight. The samples were then washed three times with 500 μl of 0.1B buffer (20 mM Tris–HCl, pH 8.0; 0.1 M KCl; 5 mM $MgCl_2$; 10% (w/v) glycerol; 0.1% (w/v) Tween 20; 10 mM β-mercaptoethanol). Elution of samples was performed by adding 20 μl of 5× SDS-PAGE sample buffer, and samples were boiled at 100 °C for 5 min.

2.4. Immunohistochemistry, immunofluorescence and electron microscopy

Brain and peripheral (sciatic) nerve sections from 2-, 7- and 20-week-old mice were analyzed ($n = 3$ for each line) by immunocytochemistry as previously described (Wang et al., 2004; Watanabe et al., 1977) using antibodies to UCH-L1 (1:4000; RA95101, Ultraclone), TH (1:1000; Chemicon) and ubiquitin (1:1000; Sigma–Aldrich, St. Louis, MO). Antibody binding was detected with 3,3′-diaminobenzidine tetrachloride (DAB) or 3-amino-9-ethylcarbazole (AEC) as a peroxidase substrate or Alexa-488- or Alexa-568-conjugated secondary antibodies (Invitrogen, Carlsbad, CA). Sections were then counterstained with hematoxylin. Ultrastructural electron microscopic studies of the substantia nigra were performed as described (Watanabe et al., 1977) using midbrain sections.

2.5. MPTP treatment

For MPTP treatment, the mice received four injections of 30 mg/kg MPTP–HCl intraperitoneally (Research Biochemicals, Natick, MA) in saline at 24-h intervals (Mochizuki et al., 2001).

2.6. Tyrosine hydroxylase-positive cell counting and biochemical analysis

Samples for both histochemistry and biochemical analysis were obtained from the same mouse. Each animal was deeply anesthetized with pentobarbital and perfused transcardially with 10 ml of ice-cold phosphate-buffered saline, and the brain was removed and divided into forebrain and midbrain–hindbrain regions.

For the tyrosine hydroxylase (TH)-positive cell counting, midbrain–hindbrain was fixed with chilled 4% formaldehyde solution (pH 7.4). The procedure of TH-positive cell counting was described previously (Furuya et al., 2004) with minor modifications. Briefly, the substantia nigra was cut into serial sections (30 μm), and every third section was subjected to immunostaining for TH using a polyclonal antibody to TH (a kind gift from I. Nagatsu, Fujita Health University, Aichi, Japan). The Vectorstain Elite ABC kit (Vector Labs, Burlingame, CA) was used for subsequent antibody detection with DAB as a peroxidase substrate. The number of viable TH-positive neurons was assessed by manual counting by a blind observer using coded slides (Furuya et al., 2004). The number of total neuronal cells outside the substantia nigra was counted after Bodian staining in the cerebral cortex (1 mm^2, seven regions per section), cerebellum (total of all lobules) and hippocampus (total number in CA1, CA2, CA3 and dentate gyrus). Statistical analysis were done by one-way ANOVA followed by post hoc test (Fisher's PLSD).

For the biochemical analysis, the striatum was quickly dissected from the forebrain, and the striatal tissue samples were weighed (~30 mg) and homogenized in 10 volumes (w/v) of ice-cold 0.05 M sodium acetate (pH 6.0). Homogenates were centrifuged (18,000 × *g*, 10 min at 4 °C), and the supernatant was frozen immediately on dry ice and stored frozen at −80 °C until use.

For the striatal dopamine measurement, supernatant (50 μl) from the striatal lysate was mixed with an equal volume of 0.2 M perchloric acid containing 0.2 mM EDTA and centrifuged (18,000 × *g*, 10 min at 4 °C), and the supernatant was applied to an HPLC system. Chromatographic separation was achieved using a C18 reversed-phase column (150 mm × 4.6 mm i.d., Model S-100; TOSOH, Tokyo, Japan). The mobile phase (50 mM citrate, 50 mM NaH_2PO_4, 0.1 mM EDTA, 4.36 mM 1-heptanesulfonate, 2.35% acetonitrile, 5.72% MeOH, pH 2.5) was pumped through the chromatographic system at a rate of 1.0 ml/min. A Coulochem electrode array system (ESA Inc., MA) with eight coulometric electrodes was used to quantify the eluted catecholamines and their metabolites. Statistical analysis was done by one-way ANOVA followed by post hoc test (Fisher's PLSD).

TH activity was assayed following the method of Hooper (1997) with minor modifications (Hooper et al., 1997; Naoi et al., 1988). The incubation mixture contained 50 μl of diluted sample and included the following components in a total volume of 200 μl: 0.2 M sodium acetate (pH 6.0), 0.2 M glycerol, 20,000 U/ml catalase, 1.0 mM 6-MPH4, 4.0 U/ml dihydropteridine reductase, 1 mM NADPH and 200 μM L-tyrosine. Incubations were carried out at 37 °C for 10 min in a shaking water bath. Reactions were terminated by adding 600 μl of ice-cold 0.33 M perchloric acid, 17 mM EDTA including 50 pmol of α-methyl DOPA as the internal standard. The L-DOPA produced was extracted onto alumina, and the catechols were eluted with 0.16 M acetic acid followed by 0.02 M phosphoric acid. A sample incubated on ice instead of 37 °C was used as a blank. The amount of L-DOPA was quantified with the HPLC system, as mentioned above. Statistical analysis was done by one-way ANOVA.

2.7. Silver staining

Sixty-micrometer brain sections from 12-week-old mice ($n = 3$ for each group) were stained using FD NeuroSilver kit (FD Neuro-Technologies, Catonsville, MD) according to the manufacturer's protocol to detect argyrophilic grain-positive degenerating neurons.

2.8. Behavioral tests

H-hI93M mice and non-Tg littermates were used for all behavioral analyses. For the accelerated rota-rod test, 20–25-week-old mice were placed on the rod (Ohara, Japan) at a speed of 5 rpm, and the speed was accelerated to 50 rpm in 5 min. The length of time that each mouse was able to remain on the rod before falling was recorded. For the locomotor activity test, 11–13-week-old or 20–23-week-old mice were placed separately in a home cage 4 days before the beginning of analysis for habituation. Two to four mice were monitored at once for locomotor activity on the home cage monitor (Ohara, Japan) for 63 h beginning from 5:30 p.m. All mice were housed with a 12 h light/dark cycle, with the light cycle beginning at 8 a.m. The last 12 h of active night were used for the analysis. Mice were weighed after the analysis; there were no differences between the weights H-hI93M and non-Tg mice (data not shown). Statistical analyses were conducted using the two-tailed Student's *t*-test.

3. Results

3.1. Generation of transgenic mice expressing human $UCHL1^{I93M}$ in neurons of the substantia nigra

The human *PDGF-B* promoter was used to drive expression of the human *UCHL1* in Tg mice (Fig. 1A) (Sasahara et al., 1991). Germline transmission of $hUCHL1^{I93M}$ was obtained in two independent Tg mouse lines (denoted L-hI93M and H-hI93M, where L and H denote low and high expression, respectively). Germline transmission of $hUCHL1^{WT}$ was obtained in one Tg mouse line (denoted hWT). The levels of transgenic mRNA and endogenous *Uchl1* mRNA were assessed by quantitative RT-PCR using primers designed to amplify specifically the *UCHL1* transgene and mouse *Uchl1*, respectively. The estimated relative expression of *UCHL1* among the transgenic lines was H-hI93M > hWT > L-hI93M. The ratio of endogenous mouse *Uchl1* transcripts to transgenic human *UCHL1* transcripts was 111 in H-hI93M, 739 in hWT and 6015 in L-hI93M ($n = 3$ for each line).

At the amino acid level, human and mouse UCH-L1 differ at only 11 discrete positions, and endogenous UCH-L1 is one of the most abundant protein in the brain. Therefore, we were not able to make distinction between the exogenous human UCH-L1 and endogenous mouse UCH-L1 in the brains of Tg mice (data not shown) using immunoblotting analysis with several antibodies against human UCH-L1 from different companies (Chemicon; UltraClone; Medac; Biogenesis). To ascertain the expression of transgene product, we used *gad* mice, which lack endogenous UCH-L1 (Saigoh et al., 1999). We mated mice

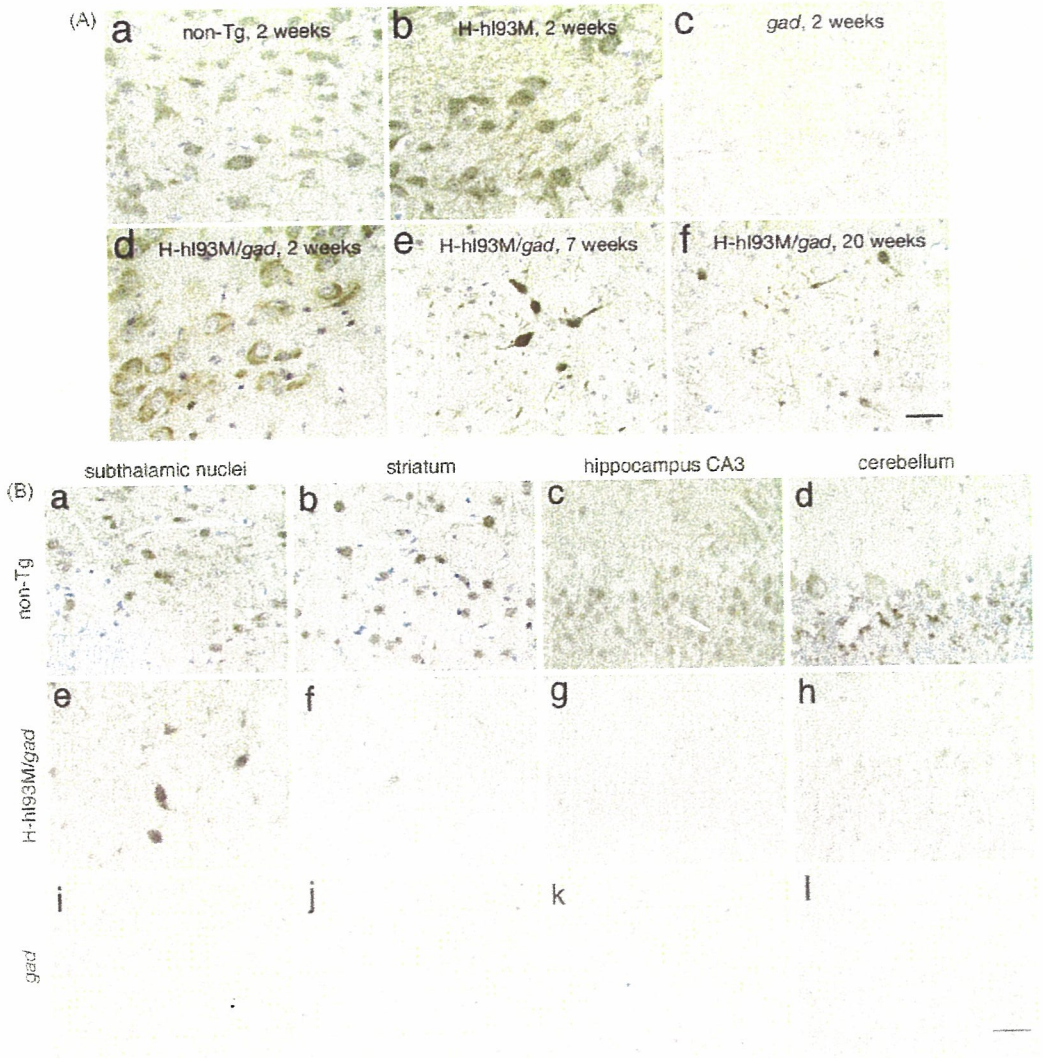

Fig. 2. Immunohistochemistry of UCH-L1 in coronal sections of the substantia nigra (A) and regions outside the substantia nigra (B) in H-hI93M. H-hI93M/*gad* and non-Tg mice. (A) Non-Tg mice (a), H-hI93M mice on a C57BL/6J background (b) and *gad* mice (c) at 2 weeks of age and H-hI93M/*gad* mice at 2 weeks (d), 7 weeks (e) and 20 weeks (f) of age. Neurons expressing UCH-L1 in the substantia nigra decreased in number and area, and densely stained neurons were observed in the aged substantia nigra. Scale bar: 30 μm. (B) UCH-L1 immunohistochemistry of coronal sections at the level of the subthalamic nuclei (a, e, i), striatum (b, f, j), hippocampus CA3 (c, g, k) and cerebellum (d, h, l). Upper row (a–d), non-Tg mice; middle row (e–h), H-hI93M/*gad* mice; lower row (i–l), *gad* mice. All mice were examined at 2 weeks of age. Scale bar: 30 μm.

from each transgenic line with mice homozygous for the *Uchl1*$^{gad/gad}$ allele (*gad* mice). Detergent-soluble (1% Triton X-100) fractions of mouse midbrain from H-hI93M/*gad* (*UCHL1*$^{I93M/-}$, *Uchl1*$^{gad/gad}$) at 2 and 15 weeks of age were subjected to SDS-PAGE and immunoblotted with anti-UCH-L1. We detected human UCH-L1 expression in H-hI93M/*gad* brains (Fig. 1B). Compared with endogenous mouse UCH-L1, which constitutes 1–2% of neuronal proteins, human UCH-L1 expression was substantially lower in H-hI93M/*gad* brains (~1% of endogenous UCH-L1 at 2 weeks of age; Fig. 1B). Interestingly, the level of transgenic human UCH-L1 was lower at 15 weeks than at 2 weeks of age (Fig. 1B). Although we could not detect human UCH-L1 in L-hI93M/*gad* and hWT/*gad* by standard immunoblotting methods, we were successful in detecting it by immunoprecipitation (Fig. 1C). These data suggest the expression of the human UCH-L1 in L-hI93M and hWT mice, which were much lower than in H-hI93M mice.

UCH-L1 is a cytosolic protein predominantly expressed in neuronal cells including dopaminergic neurons at substantia nigra with diffuse localization (data not shown). Thus, we next examined the immunohistochemical localization of the transgene products. In agreement with the data obtained by Western blotting analysis, UCH-L1-immunoreactive cells were not observed in any brain region, including the substantia nigra, of the L-hI93M/*gad* and hWT/*gad* mice (data not shown). In H-hI93M/*gad* mice, however, human UCH-L1^{I93M} was detected in the substantia nigra, the region that contains the central pathological lesions in PD, with relatively high intensities (Fig. 2A). Subthalamic nuclei, striatum, hippocampus CA3 and cerebellum also contained UCH-L1 immunoreactive cells in H-hI93M/*gad* mice (Fig. 2B). As with the previous report that CAT expression under control of the *PDGF-B* promoter in transgenic mice localizes to neuronal cell bodies (Sasahara et al., 1991), most UCH-L1-immunoreactive cells in H-hI93M/*gad* mice had a neuronal morphology (Fig. 2). Western blotting analysis of midbrain lysates showed a reduction of transgenic UCH-L1^{I93M} at 15 weeks of age as compared with that at 2 weeks in H-hI93M/*gad* mice (Fig. 1B). Thus, we also performed immunohistochemical analysis of UCH-L1 on substantia nigra from 2-, 7- and 20-week-old H-hI93M/*gad* mice. We found many UCH-L1-positive neurons at 2 weeks. The number of positive cells had decreased by 7 weeks, however, at which time small-sized and densely stained neurons were observed, and UCH-L1-positive cells were barely

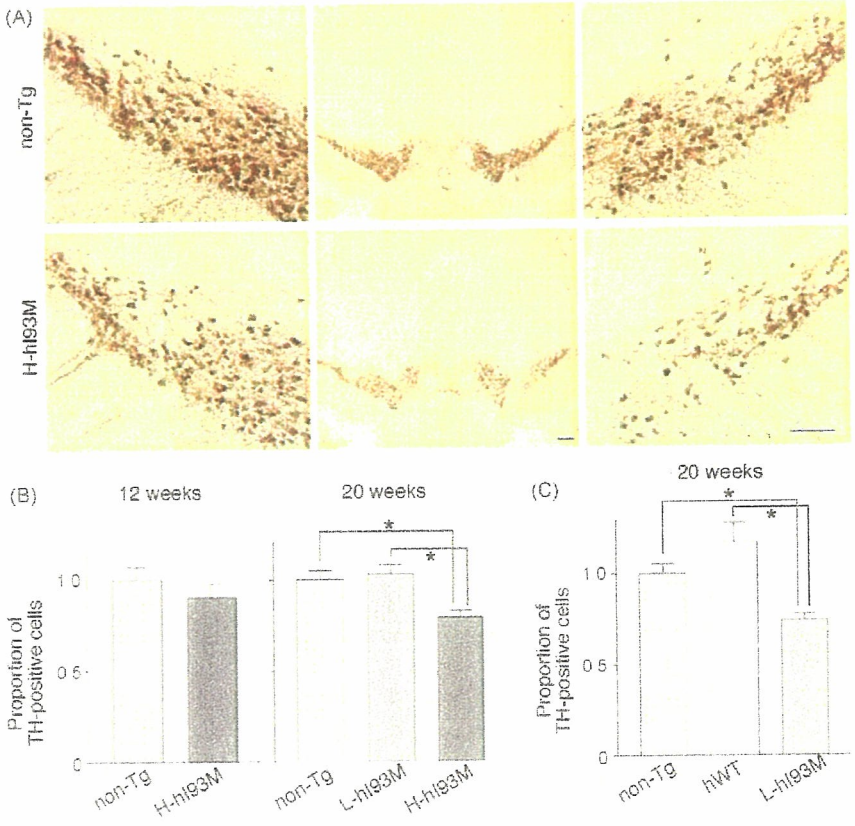

Fig. 3. TH-positive neurons of hI93M Tg mice were reduced as the animals aged. (A) Immunohistochemical staining of the substantia nigra with anti-TH in non-Tg (upper panels) and H-hI93M (lower panels) mice at 20 weeks of age. Scale bar: 1 mm. Left and right panels in the figure correspond to the left and right part of the middle panel, respectively. (B) Proportion of neurons stained with anti-TH in the substantia nigra from non-Tg and hI93M mice at 12 weeks (left panel) and 20 weeks (right panel) of age. Cell numbers were normalized to those for the non-Tg mice. Values are the mean ± S.E.M.; $n = 10$ Significance was examined by a one-way ANOVA. $^{*}p < 0.01$. (C) The number of TH-positive cells in the substantia nigra from 20-week-old non-Tg ($n = 5$). hWT ($n = 3$) and L-hI93M mice ($n = 5$) after treatment with MPTP. The cell numbers were normalized to those for non-Tg mice. Values are the mean ± S.E.M. Significance was examined by a one-way ANOVA. $^{*}p < 0.001$.

detectable at 20 weeks of age (Fig. 2A). Together, our results indicate that hUCH-L1^{I93M} is expressed in the neurons of the substantia nigra in H-hI93M mice, but the number of positive cells declines before 20 weeks of age. With the failure to detect hUCH-L1 protein in hWT/*gad* mice and L-hI93M/*gad* mice both in the Western blotting and the immunohistochemistry, we performed most of the analysis using H-hI93M mice with non-Tg mice as a control.

3.2. Loss of dopaminergic neurons in the substantia nigra of 20-week-old H-hI93M mice

We next determined whether the number of midbrain dopaminergic neurons was reduced in the substantia nigra of transgenic mice using TH immunohistochemistry. The number of TH-positive dopaminergic neurons in the substantia nigra at the same neuroanatomical level was compared and quantified for each transgenic mouse line. Surprisingly, we detected an ~30% reduction in TH-positive neurons in 20-week-old H-hI93M mice as compared with those in non-Tg control mice (Fig. 3A and B). This reduction was not seen in 12-week-old H-hI93M mice or 20-week-old L-hI93M mice. Together with the decrease in the level of UCH-L1^{I93M} (Fig. 1B) and the reduction in UCH-L1-positive neurons in the substantia nigra of H-hI93M/*gad* mice, our data indicate that UCH-L1^{I93M} expression in the dopaminergic neurons is sufficient to induce the degeneration of these neurons.

MPTP is a toxin used to induce an acute Parkinsonian syndrome that is indistinguishable from sporadic PD (Dauer and Przedborski, 2003). MPTP metabolite 1-methyl-4-pyridinium (MPP^+), an inhibitor of complex I of the mitochondrial respiration chain, is taken up by the terminals of dopaminergic neurons via the dopamine transporter (DAT), thereby causing the selective death of nigral neurons (Dauer and Przedborski, 2003). Although neuronal loss was not observed in L-hI93M mice at 20 weeks of age, we speculated that dopaminergic

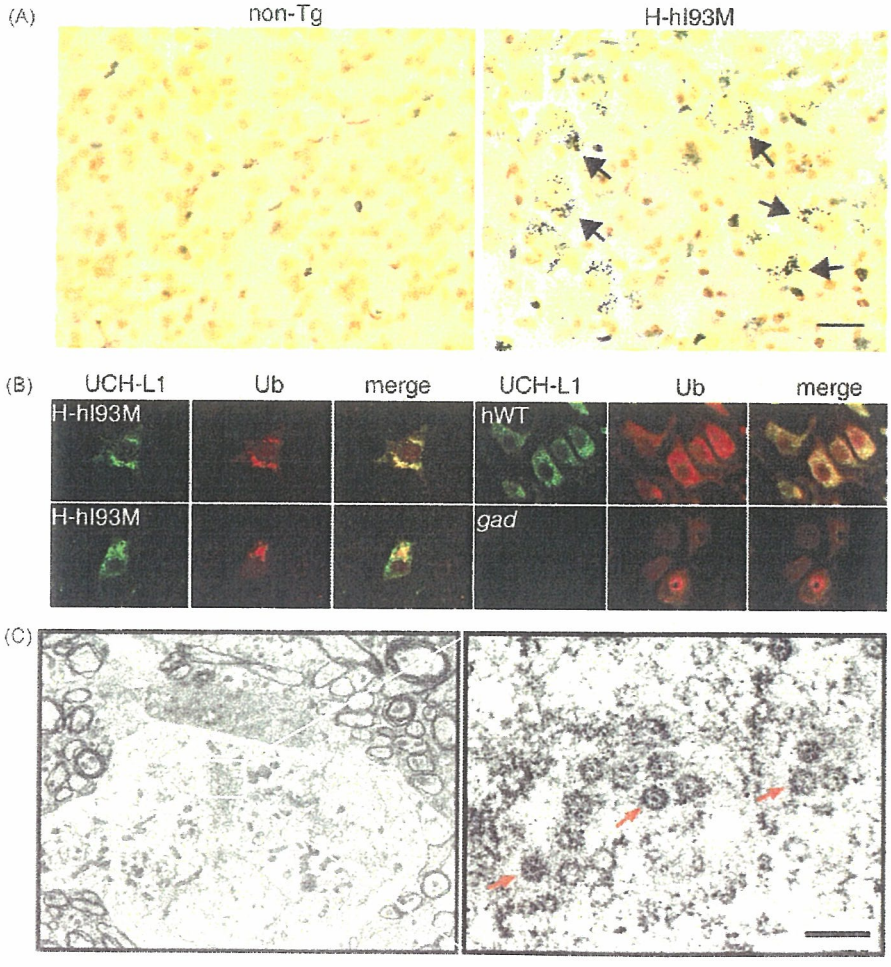

Fig. 4. Several neuropathological features reminiscent of PD are present in H-hI93M mice brains. (A) Silver staining of the substantia nigra at 12 weeks of age in non-Tg and H-hI93M mice. Note the presence of silver staining-positive argyrophilic grains in the cell bodies of some dopaminergic neurons in H-hI93M mice (arrows). This kind of abnormal structure was not seen in substantia nigra of non-Tg mice. Scale bar: 30 μm. (B) Confocal images of dopaminergic neurons from hWT, H-hI93M and *gad* mice. H-hI93M mice showed the formation of ubiquitin-positive cytoplasmic inclusions (red) co-localized with UCH-L1 staining (green) in the remaining nigral neurons at 20 weeks of age. Compared with the diffuse, reduced staining of ubiquitin in *gad* mice, nigral neurons from hWT mice also showed a diffuse pattern of staining but with fine small granular cytoplasmic staining (red) co-localized with UCH-L1 (green). (C) Electron micrographs of a nigral neuron from a 20-week-old H-hI93M mouse at the level of the cell body (left panel), and dense-core vesicles (red arrows) at higher magnification (right panel). Scale bar: 1 μm.

neurons of L-hI93M mice might be more susceptible to MPTP toxin compared to that of non-Tg mice or hWT mice. As expected, significantly fewer TH-positive neurons were observed in L-hI93M mice after MPTP treatment as compared with hWT or non-Tg control mice though hWT express higher *hUCHL1* compared to L-hI93M (Fig. 3C). The number of TH-positive neurons in MPTP-treated hWT mice was somewhat higher than that in non-Tg mice ($p < 0.001$). Taken together with the fact that expression of human UCH-L1 in L-hI93M is lower than that in hWT, these results suggest that the UCH-L1^{I93M} mutant, but not UCH-L1^{WT}, is specifically toxic to dopaminergic neurons.

3.3. Presence of neuropathology in dopaminergic neurons from H-hI93M mice

To evaluate the degenerative process of dopaminergic neurons, silver staining was used to indicate argyrophilic degenerating neurons (Lo Bianco et al., 2004). In non-Tg mice, no silver staining was observed, whereas scattered neurons containing grains that were silver staining positive were present in the substantia nigra of H-hI93M mice (Fig. 4A). The presence of intracellular inclusions called Lewy bodies and Lewy neurites are neuropathological characteristics of PD and are silver staining positive (Sandmann-Keil et al., 1999; Uchihara et al., 2005). It is also known that UCH-L1 and ubiquitin, as well as α-synuclein, are components of Lewy bodies (Lowe et al., 1990). Furthermore, UCH-L1 is tightly associated with mono-ubiquitin *in vivo* (Osaka et al., 2003). Thus, we expected that the silver staining-positive grains might have characteristic features of Lewy bodies. We therefore compared the immunohistochemical analysis of UCH-L1 and ubiquitin. Compared with reduced staining for ubiquitin in *gad* mice, strong and diffuse ubiquitin staining was observed in nigral neurons of hWT mice and non-Tg mice (data not shown), and this staining co-localized with UCH-L1, which is in agreement with our previous report (Osaka et al., 2003). In H-hI93M substantia nigra at 20 weeks of age, ubiquitin- and UCH-L1-positive cytoplasmic inclusions, a large aggregates with different morphology from small dots usually seen in hWT mice and non-Tg mice, were observed in a portion of the remaining nigral neurons (Fig. 4B). These inclusions were, however, α-synuclein or hematoxylin–eosin (HE) negative (data not shown). We could not observe UCH-L1- and ubiquitin-positive inclusions in L-hI93M mice (data not shown).

Another cellular characteristic of PD neuropathology is dense-core vesicles of about 80–200 nm in perikarya, which are frequently observed along with Lewy bodies in PD patients (Watanabe et al., 1977). We observed electron dense-core vesicles in the cytoplasm of ~30% of nigral neurons in H-hI93M mice using electron microscopy (Fig. 4C). In non-Tg mice, such vesicles with a similar shape were not detected in cell bodies but rather were seen in synaptic terminals. Taken together, our data indicate that degenerating dopaminergic neurons in the substantia nigra of H-hI93M mice are devoid of Lewy bodies but show some neuropathological features such as silver staining-positive argyrophilic grains, aggregates with UCH-L1 and ubiquitin, and dense-core vesicles in the perikarya.

3.4. Increased amount of SDS-insoluble but urea/SDS-soluble UCH-L1 in the midbrain of H-hI93M mice

UCH-L1^{I93M} has reduced α-helical content as compared with UCH-L1^{WT} (Nishikawa et al., 2003), and UCH-L1^{I93M} overexpression in COS7 cells results in more cells that contain cytoplasmic inclusions (Ardley et al., 2004). Thus, the presence of UCH-L1-positive inclusions in H-hI93M dopaminergic neurons led us to speculate whether UCH-L1^{I93M} would be less soluble than the wild-type protein *in vivo*. To biochemically characterize the changes in UCH-L1 deposited in the brains of H-hI93M mice, we sequentially extracted frozen midbrain tissues with 5% SDS (soluble fraction) and 8 M urea/5% SDS (insoluble fraction) and analyzed each fraction by immunoblotting with anti-UCH-L1. As expected, immunoblots of insoluble fractions showed a modest but statistically significant increase in UCH-L1 in the midbrains of H-hI93M mice as compared with those from a non-Tg mouse (Fig. 5A and B), indicating increased insolubility of UCH-L1^{I93M} *in vivo*, which might have resulted in dopaminergic neurotoxicity.

3.5. Decreased dopamine content in the striata of H-hI93M mice

Because the nigro-striatal pathway is severely affected in PD patients, and because our mice showed the degeneration of dopaminergic neurons in the substantia nigra, we evaluated the nerve terminals in the striatal pathway using

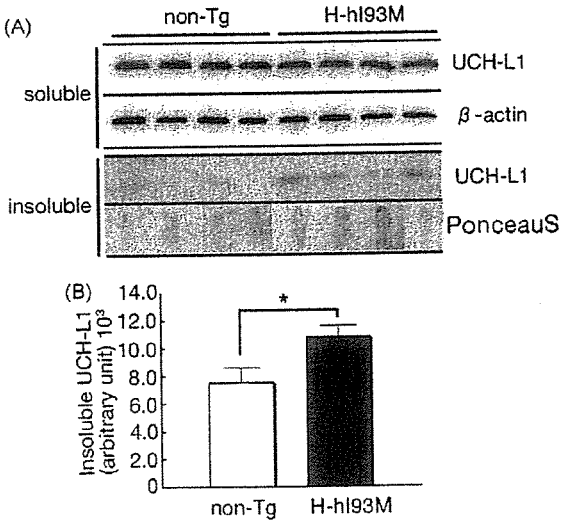

Fig. 5. Protein insolubility of UCH-L1 in H-hI93M Tg mice. (A) Immunoblotting analysis of UCH-L1 in soluble (5% SDS soluble) and insoluble (5% SDS insoluble and 8 M urea/5% SDS soluble) fractions from tissue containing the substantia nigra (11–13 weeks). Soluble fraction (5 μg for each) was probed with anti-UCH-L1 or anti-β-actin. Insoluble fraction (0.5 μg for each) was probed with anti-UCH-L1. One microgram of each insoluble fraction was applied to dot blotting and stained by Ponceau S to show that each fraction contained the same amount of total protein. A slight increase in the insolubility of UCH-L1 in the substantia nigra fraction from H-hI93M mice is seen as compared with that from non-Tg mice. (B) The experiment was done with H-hI93M mice and non-Tg littermates from five different litters, and the results of quantitative analyses in insoluble fraction is shown ($n = 5$ mice for each group).

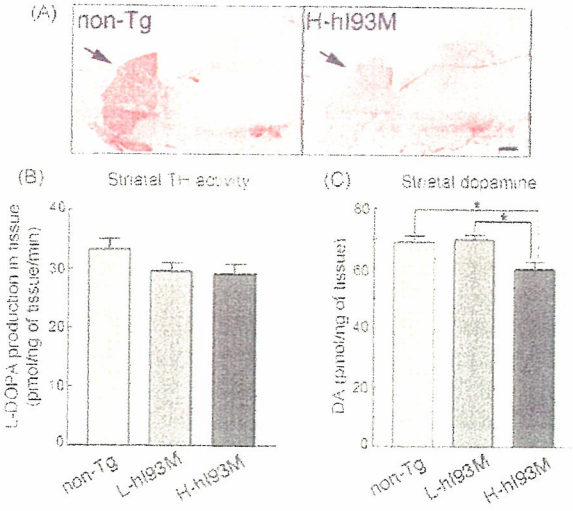

Fig. 6. H-hI93M mice show pathology in the striatum. Dopamine content and TH activity were lower in H-hI93M mice. (A) Sagittal sections from non-Tg and H-hI93M mice at 20 weeks of age were immunostained with the dopaminergic marker anti-TH. TH immunoreactivity is decreased in the nigro-striatal axons (arrows) of H-hI93M brains. Scale bar: 100 μm. (B) TH activity and (C) dopamine content were measured following extraction and homogenization of the mouse striatum of non-Tg, L-hI93M and H-hI93M mice at 20 weeks of age ($n = 4$; mean ± S.E). Significance was examined by a one-way ANOVA. $^{*}p < 0.05$.

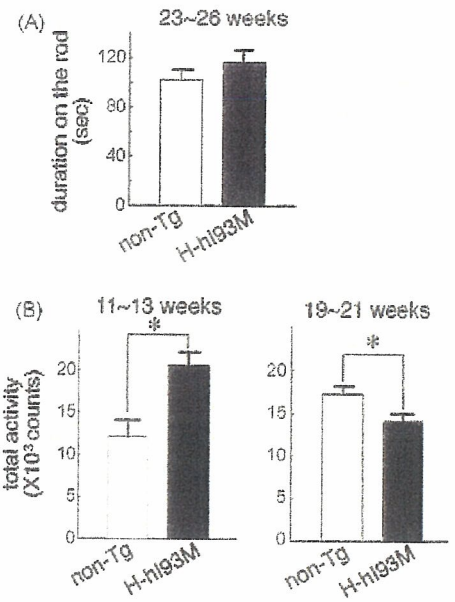

Fig. 7. H-hI93M transgenic mice show locomotor deficits. (A) Accelerated rota-rod analysis of H-hI93M and non-Tg mice ($n = 6$ for non-Tg and $n = 7$ for H-hI93M) at 23–26 weeks of age. Mice were placed on a rod, and their duration on the rod before falling off (mean value of three trials for each animal) was recorded. (B) Home cage monitor analysis of H-hI93M and non-Tg mice at 11–13 weeks of age (left; $n = 4$ for each line) and at 19–21 weeks of age (right; $n = 8$ for non-Tg and $n = 10$ for H-hI93M). Note the significant hypolocomotion of H-hI93M mice as compared with non-Tg mice at 19–21 weeks of age. Values are the mean ± S.E.M. Significance was examined using the unpaired Student's t-test. $^{*}p < 0.05$.

immunohistochemical and biochemical analyses. In agreement with the reduction of TH-positive dopaminergic neurons in the substantia nigra, nigro-striatal fibers in H-hI93M mice showed decreased immunoreactivity for TH as compared with that of non-Tg mice (Fig. 6A). TH activity, analyzed by determining L-DOPA production in the striatal tissues, also showed a tendency to decline in H-hI93M mice, although it was not significantly different (Fig. 6B). Loss of dopaminergic neurons in the substantia nigra and decreased TH activity in the striatum of H-hI93M mice prompted us to examine the concentration of striatal dopamine. Compared with non-Tg mice, H-hI93M mice showed a significant reduction of dopamine content in the striatum (Fig. 6C).

3.6. Decreased spontaneous, voluntary movements of H-hI93M mice

Given the prominent loss of dopaminergic neurons in the substantia nigra and the reduction in dopamine content in the striatum of H-hI93M mice, we next assessed the locomotor abilities of H-hI93M mice using a battery of well-established behavioral tests. Involuntary movement was analyzed by the rota-rod test (Goldberg et al., 2005) on 23–26-week-old mice. H-hI93M mice and non-Tg mice were similarly able to maintain their balance on the rotating rod during rod acceleration before falling off (Fig. 7A). We next analyzed spontaneous, voluntary movements with a locomotor activity test (Goldberg et al., 2005). Unexpectedly, 11–13-week-old H-hI93M mice showed significant hyperlocomotion during active periods (i.e., at night) as compared with non-Tg mice during home cage monitoring (Fig. 7B). However, 19–21-week-old H-hI93M mice showed a modest but significant reduction in locomotor activity during active periods as compared with non-Tg mice (Fig. 7B). These results indicate that, in addition to the neuropathological changes, H-hI93M mice exhibit mild behavioral deficits related to PD.

4. Discussion

In this study, we characterized transgenic mice expressing hUCH-L1^{I93M}, a mutation with presumptive association with familial PD, in the brain. Our previous attempt of making mouse UCH-L1^{WT} Tg mice under various higher expressing promoters, such as EF1α, resulted in an infertility of mice, thus it was impossible to maintain the lines. This failure resulted from the effect of overexpressing UCH-L1 in the testis/ovary leading to an increased apoptosis in these reproductive organs, although we did not find obvious morphological differences in the brain (Wang et al., 2006). Thus, we used *PDGF-B* promoter in this study to avoid massive expression of the transgene.

Two lines of hUCH-L1^{I93M} Tg mice and one line of hUCH-L1^{WT} Tg mice were viable and fertile without any predictable abnormalities. All of the three Tg lines expressed very limited levels of the human *UCHL1* gene with a maximum transcript ratio of about 1/100 as compared with the endogenous mouse *Uchl1*. However, immunohistological analysis indicated that higher level of hUCH-L1^{I93M} expression could be detected in the large number of neurons in the substantia nigra of

H-hI93M/gad mice at 2 weeks of age. In addition, there is a difference in the morphology of hUCH-L1^{I93M} expressing neurons, reminiscent of dying neurons, in the substantia nigra of H-hI93M/gad mice among 7 and 20 weeks of age. We also observed an eventual decline in the number of UCH-L1-positive neurons in H-hI93M/gad mice, as they age. Furthermore, the dopaminergic neurons in the substantia nigra of H-hI93M mice at 12 weeks of age showed silver staining-positive argylophilic grains, which represent neurons undergoing degeneration (Lo Bianco et al., 2004). Since we observed a loss of dopaminergic neurons in the substantia nigra and reduced dopamine content in the striatum of H-hI93M mice at 20 weeks of age, our results indicate the possibility that hUCH-L1^{I93M} expressing dopaminergic neurons degenerate with age.

In addition to cell loss, several neuropathological features were observed in the substantia nigra of H-hI93M mice. Dopaminergic neurons had (1) electron dense-core vesicles in the perikarya, and (2) cytoplasmic inclusions that were positive for both UCH-L1 and ubiquitin. Despite these features, we did not observe eosinophilic or α-synuclein-positive Lewy bodies at the substantia nigra in our morphological analyses. Thus, the mouse dopaminergic neurons expressing UCH-L1^{I93M} may die prior to the formation of Lewy bodies, or those mice might form these structures at stages beyond the period of our study.

The mechanisms responsible for dopaminergic cell loss in the substantia nigra of H-hI93M mice remain elusive. The I93M mutation in UCH-L1 reduces its hydrolase activity by about 50%, which has been suggested as a cause for the pathogenesis of PD (Nishikawa et al., 2003). However, we have not found clear evidence for nigro-striatal dopaminergic pathology in *gad* mice (data not shown). Since expression of UCH-L1 is not detected in gad mice, the reduction of hydrolase activity alone would not be the cause of PD. In light of our finding here that transgenic expression of UCH-L1^{I93M} results in dopaminergic pathology in mice, it would seem that this mutation elicits a gain of toxic function leading to the neuronal toxicity in the substantia nigra.

Our previous work using circular dichroism suggests that the I93M mutation reduces the α-helical content of UCH-L1 (Nishikawa et al., 2003). Recently, we had also showed, using small-angle neutron scattering, that wild-type or I93M mutant UCH-L1 exists as a dimmer in an aqueous solution. Moreover, their configuration differed; wild-type UCH-L1 has ellipsoidal shape where as I93M mutant has more globular shape (Naito et al., 2006). Cells expressing UCH-L1^{I93M} are more prone to form inclusions (Ardley et al., 2004). Proteomic analysis of autopsied brains from PD patients and AD patients shows that UCH-L1 is extensively modified by carbonyl formation, methionine oxidation and cysteine oxidation in the diseased brains (Choi et al., 2004). These modifications are shown to result from oxidative stress (Choi et al., 2004). We show here that I93M mutation in UCH-L1 increases its insolubility *in vivo*. From the very limited expression of human UCH-L1 I93M, it is possible to speculate that endogenous mouse UCH-L1 might become insoluble in the presence of I93M UCH-L1. In addition, L-hI93M neurons were more susceptible than hWT or non-Tg neurons to MPTP, an inhibitor of complex I. This observation suggests that UCH-L1^{I93M} easily gains toxicity under oxidative stress. The conformational change and/or the additional methionine oxidation in UCH-L1 caused by I93M mutation may cause increased insolubility and lead to the gain of a toxic function.

In addition, our behavioral analysis revealed that H-hI93M mice exhibit very slight defects in spontaneous, voluntary movement, as shown by their hyperlocomotion at 11–13 weeks of age and by their hypolocomotion at 19–21 weeks of age in the home cage monitor test. Patients with PD exhibit no clinical symptoms until 70–80% of dopaminergic neurons are lost (Dauer and Przedborski, 2003). Thus, the level of dopaminergic neuronal loss seen in H-hI93M mice might not be sufficient to produce severe clinical phenotypes. It is difficult to explain the hyperlocomotion detected at 11–13 weeks of age, by simple changes in the nigro-striatal pathway. Other brain areas might be related to the locomotor changes seen in H-hI93M mice. We will need further analysis to connect the dopaminergic cell loss and defects in spontaneous, voluntary movement in H-hI93M mice.

In attempts to replicate neuropathological aspects of PD, several of the familial PD genes have been altered in mice. Up to date, α-synuclein Tg mice with or without mutation (Fernagut and Chesselet, 2004), parkin knockout mice (Goldberg et al., 2003; Itier et al., 2003; Palacino et al., 2004; Perez and Palmiter, 2005; Von Coelln et al., 2004), and DJ-1 knockout mice (Chen et al., 2005; Goldberg et al., 2005; Kim et al., 2005) have been reported. Although these mice show some alterations in the function of dopaminergic neurons, none has dopaminergic neuron loss in the substantia nigra. Thus, we have developed the first mouse model with an alteration in a familial PD gene that leads to dopaminergic cell loss. Further analysis of these mice will help establish the role of UCH-L1 in PD, which may elucidate a common pathway for both familial and sporadic PD.

Acknowledgements

This work was supported by the Program for Promotion of Fundamental Studies in Health Sciences of the National Institute of Biomedical Innovation of Japan (KW); Grants-in-Aid for Scientific Research from the Ministry of Health, Labour and Welfare of Japan (KW); Grants-in-Aid for Scientific Research from the Ministry of Education, Culture, Sports, Science and Technology of Japan (KW); a grant from Japan Science and Technology Cooperation and a High Technology Research Center Grant (YM). We thank M. Shikama for the care and breeding of animals, H. Fujita for genotyping of animals, H. Kikuchi for technical assistance with tissue sections and N. Takagaki for the support in English. We also thank Dr. H. Hohjo for letting us use the home cage monitor.

References

Aoki, S., Su, Q., Li, H., Nishikawa, K., Ayukawa, K., Hara, Y., Namikawa, K., Kiryu-Seo, S., Kiyama, H., Wada, K., 2002. Identification of an axotomy-induced glycosylated protein, AIGP1, possibly involved in cell death triggered by endoplasmic reticulum-Golgi stress. J. Neurosci. 22, 10751–10760.

Ardley, H.C., Scott, G.B., Rose, S.A., Tan, N.G., Robinson, P.A., 2004. UCH-L1 aggresome formation in response to proteasome impairment indicates a role in inclusion formation in Parkinson's disease. J. Neurochem. 90, 379–391.

Bonifati, V., Rizzu, P., van Baren, M.J., Schaap, O., Breedveld, G.J., Krieger, E., Dekker, M.C., Squitieri, F., Ibanez, P., Joosse, M., van Dongen, J.W., Vanacore, N., van Swieten, J.C., Brice, A., Meco, G., van Duijn, C.M., Oostra, B.A., Heutink, P., 2003. Mutations in the DJ-1 gene associated with autosomal recessive early-onset parkinsonism. Science 299, 256–259.

Chartier-Harlin, M.C., Kachergus, J., Roumier, C., Mouroux, V., Douay, X., Lincoln, S., Levecque, C., Larvor, L., Andrieux, J., Hulihan, M., Waucquier, N., Defebvre, L., Amouyel, P., Farrer, M., Destee, A., 2004. Alpha-synuclein locus duplication as a cause of familial Parkinson's disease. Lancet 364, 1167–1169.

Chen, L., Cagniard, B., Mathews, T., Jones, S., Koh, H.C., Ding, Y., Carvey, P.M., Ling, Z., Kang, U.J., Zhuang, X., 2005. Age-dependent motor deficits and dopaminergic dysfunction in DJ-1 null mice. J. Biol. Chem. 280, 21418–21426.

Choi, J., Levey, A.I., Weintraub, S.T., Rees, H.D., Gearing, M., Chin, L.S., Li, L., 2004. Oxidative modifications and down-regulation of ubiquitin carboxyl-terminal hydrolase L1 associated with idiopathic Parkinson's and Alzheimer's diseases. J. Biol. Chem. 279, 13256–13264.

Dauer, W., Przedborski, S., 2003. Parkinson's disease: mechanisms and models. Neuron 39, 889–909.

Farrer, M., Kachergus, J., Forno, L., Lincoln, S., Wang, D.S., Hulihan, M., Maraganore, D., Gwinn-Hardy, K., Wszolek, Z., Dickson, D., Langston, J.W., 2004. Comparison of kindreds with parkinsonism and alpha-synuclein genomic multiplications. Ann. Neurol. 55, 174–179.

Fernagut, P.O., Chesselet, M.F., 2004. Alpha-synuclein and transgenic mouse models. Neurobiol. Dis. 17, 123–130.

Furuya, T., Hayakawa, H., Yamada, M., Yoshimi, K., Hisahara, S., Miura, M., Mizuno, Y., Mochizuki, H., 2004. Caspase-11 mediates inflammatory dopaminergic cell death in the 1-methyl-4-phenyl-1,2,3,6-tetrahydropyridine mouse model of Parkinson's disease. J. Neurosci. 24, 1865–1872.

Goldberg, M.S., Fleming, S.M., Palacino, J.J., Cepeda, C., Lam, H.A., Bhatnagar, A., Meloni, E.G., Wu, N., Ackerson, L.C., Klapstein, G.J., Gajendiran, M., Roth, B.L., Chesselet, M.F., Maidment, N.T., Levine, M.S., Shen, J., 2003. Parkin-deficient mice exhibit nigrostriatal deficits but not loss of dopaminergic neurons. J. Biol. Chem. 278, 43628–43635.

Goldberg, M.S., Pisani, A., Haburcak, M., Vortherms, T.A., Kitada, T., Costa, C., Tong, Y., Martella, G., Tscherter, A., Martins, A., Bernardi, G., Roth, B.L., Pothos, E.N., Calabresi, P., Shen, J., 2005. Nigrostriatal dopaminergic deficits and hypokinesia caused by inactivation of the familial Parkinsonism-linked gene DJ-1. Neuron 45, 489–496.

Hemelaar, J., Borodovsky, A., Kessler, B.M., Reverter, D., Cook, J., Kolli, N., Gan-Erdene, T., Wilkinson, K.D., Gill, G., Lima, C.D., Ploegh, H.L., Ovaa, H., 2004. Specific and covalent targeting of conjugating and deconjugating enzymes of ubiquitin-like proteins. Mol. Cell. Biol. 24, 84–95.

Hooper, D., Kawamura, M., Hoffman, B., Kopin, I.J., Hunyady, B., Mezey, E., Eisenhofer, G., 1997. Tyrosine hydroxylase assay for detection of low levels of enzyme activity in peripheral tissues. J. Chromatogr. B: Biomed. Sci. Appl. 694, 317–324.

Ibanez, P., Bonnet, A.M., Debarges, B., Lohmann, E., Tison, F., Pollak, P., Agid, Y., Durr, A., Brice, A., 2004. Causal relation between alpha-synuclein gene duplication and familial Parkinson's disease. Lancet 364, 1169–1171.

Itier, J.M., Ibanez, P., Mena, M.A., Abbas, N., Cohen-Salmon, C., Bohme, G.A., Laville, M., Pratt, J., Corti, O., Pradier, L., Ret, G., Joubert, C., Periquet, M., Araujo, F., Negroni, J., Casarejos, M.J., Canals, S., Solano, R., Serrano, A., Gallego, E., Sanchez, M., Denefle, P., Benavides, J., Tremp, G., Rooney, T.A., Brice, A., Garcia de Yebenes, J., 2003. Parkin gene inactivation alters behaviour and dopamine neurotransmission in the mouse. Hum. Mol. Genet. 12, 2277–2291.

Kahle, P.J., Neumann, M., Ozmen, L., Muller, V., Odoy, S., Okamoto, N., Jacobsen, H., Iwatsubo, T., Trojanowski, J.Q., Takahashi, H., Wakabayashi, K., Bogdanovic, N., Riederer, P., Kretzschmar, H.A., Haass, C., 2001. Selective insolubility of alpha-synuclein in human Lewy body diseases is recapitulated in a transgenic mouse model. Am. J. Pathol. 159, 2215–2225.

Kim, R.H., Smith, P.D., Aleyasin, H., Hayley, S., Mount, M.P., Pownall, S., Wakeham, A., You-Ten, A.J., Kalia, S.K., Horne, P., Westaway, D., Lozano, A.M., Anisman, H., Park, D.S., Mak, T.W., 2005. Hypersensitivity of DJ-1-deficient mice to 1-methyl-4-phenyl-1,2,3,6-tetrahydropyrindine (MPTP) and oxidative stress. Proc. Natl. Acad. Sci. U.S.A. 102, 5215–5220.

Kitada, T., Asakawa, S., Hattori, N., Matsumine, H., Yamamura, Y., Minoshima, S., Yokochi, M., Mizuno, Y., Shimizu, N., 1998. Mutations in the parkin gene cause autosomal recessive juvenile parkinsonism. Nature 392, 605–608.

Kruger, R., Kuhn, W., Muller, T., Woitalla, D., Graeber, M., Kosel, S., Przuntek, H., Epplen, J.T., Schols, L., Riess, O., 1998. Ala30Pro mutation in the gene encoding alpha-synuclein in Parkinson's disease. Nat. Genet. 18, 106–108.

Larsen, C.N., Krantz, B.A., Wilkinson, K.D., 1998. Substrate specificity of deubiquitinating enzymes: ubiquitin C-terminal hydrolases. Biochemistry 37, 3358–3368.

Leroy, E., Boyer, R., Auburger, G., Leube, B., Ulm, G., Mezey, E., Harta, G., Brownstein, M.J., Jonnalagada, S., Chernova, T., Dehejia, A., Lavedan, C., Gasser, T., Steinbach, P.J., Wilkinson, K.D., Polymeropoulos, M.H., 1998. The ubiquitin pathway in Parkinson's disease. Nature 395, 451–452.

Lincoln, S., Vaughan, J., Wood, N., Baker, M., Adamson, J., Gwinn-Hardy, K., Lynch, T., Hardy, J., Farrer, M., 1999. Low frequency of pathogenic mutations in the ubiquitin carboxy-terminal hydrolase gene in familial Parkinson's disease. Neuroreport 10, 427–429.

Liu, Y., Fallon, L., Lashuel, H.A., Liu, Z., Lansbury Jr., P.T., 2002. The UCH-L1 gene encodes two opposing enzymatic activities that affect alpha-synuclein degradation and Parkinson's disease susceptibility. Cell 111, 209–218.

Lo Bianco, C., Schneider, B.L., Bauer, M., Sajadi, A., Brice, A., Iwatsubo, T., Aebischer, P., 2004. Lentiviral vector delivery of parkin prevents dopaminergic degeneration in an alpha-synuclein rat model of Parkinson's disease. Proc. Natl. Acad. Sci. U.S.A. 101, 17510–17515.

Lowe, J., McDermott, H., Landon, M., Mayer, R.J., Wilkinson, K.D., 1990. Ubiquitin carboxyl-terminal hydrolase (PGP 9.5) is selectively present in ubiquitinated inclusion bodies characteristic of human neurodegenerative diseases. J. Pathol. 161, 153–160.

Maraganore, D.M., Farrer, M.J., Hardy, J.A., Lincoln, S.J., McDonnell, S.K., Rocca, W.A., 1999. Case-control study of the ubiquitin carboxy-terminal hydrolase L1 gene in Parkinson's disease. Neurology 53, 1858–1860.

Mochizuki, H., Hayakawa, H., Migita, M., Shibata, M., Tanaka, R., Suzuki, A., Shimo-Nakanishi, Y., Urabe, T., Yamada, M., Tamayose, K., Shimada, T., Miura, M., Mizuno, Y., 2001. An AAV-derived Apaf-1 dominant negative inhibitor prevents MPTP toxicity as antiapoptotic gene therapy for Parkinson's disease. Proc. Natl. Acad. Sci. U.S.A. 98, 10918–10923.

Naito, S., Mochizuki, H., Yasuda, T., Mizuno, Y., Furusaka, M., Ikeda, S., Adachi, T., Shimizu, H.M., Suzuki, J., Fujiwara, S., Okada, T., Nishikawa, K., Aoki, S., Wada, K., 2006. Characterization of multimetric variants of ubiquitin carboxyl-terminal hydrolase L1 in water by small-angle neutron scattering. Biochem. Biophys. Res. Commun. 339, 717–725.

Naoi, M., Takahashi, T., Nagatsu, T., 1988. Simple assay procedure for tyrosine hydroxylase activity by high-performance liquid chromatography employing coulometric detection with minimal sample preparation. J. Chromatogr. 427, 229–238.

Nishikawa, K., Li, H., Kawamura, R., Osaka, H., Wang, Y.L., Hara, Y., Hirokawa, T., Manago, Y., Amano, T., Noda, M., Aoki, S., Wada, K., 2003. Alterations of structure and hydrolase activity of parkinsonism-associated human ubiquitin carboxyl-terminal hydrolase L1 variants. Biochem. Biophys. Res. Commun. 304, 176–183.

Osaka, H., Wang, Y.L., Takada, K., Takizawa, S., Setsuie, R., Li, H., Sato, Y., Nishikawa, K., Sun, Y.J., Sakurai, M., Harada, T., Hara, Y., Kimura, I., Chiba, S., Namikawa, K., Kiyama, H., Noda, M., Aoki, S., Wada, K., 2003. Ubiquitin carboxy-terminal hydrolase L1 binds to and stabilizes monoubiquitin in neuron. Hum. Mol. Genet. 12, 1945–1958.

Paisan-Ruiz, C., Jain, S., Evans, E.W., Gilks, W.P., Simon, J., van der Brug, M., Lopez de Munain, A., Aparicio, S., Gil, A.M., Khan, N., Johnson, J., Martinez, J.R., Nicholl, D., Carrera, I.M., Pena, A.S., de Silva, R., Lees, A., Marti-Masso, J.F., Perez-Tur, J., Wood, N.W., Singleton, A.B., 2004. Cloning of the gene containing mutations that cause PARK8-linked Parkinson's disease. Neuron 44, 595–600.

Palacino, J.J., Sagi, D., Goldberg, M.S., Krauss, S., Motz, C., Wacker, M., Klose, J., Shen, J., 2004. Mitochondrial dysfunction and oxidative damage in parkin-deficient mice. J. Biol. Chem. 279, 18614–18622.

Perez, F.A., Palmiter, R.D., 2005. Parkin-deficient mice are not a robust model of parkinsonism. Proc. Natl. Acad. Sci. U.S.A. 102, 2174–2179.

Polymeropoulos, M.H., Lavedan, C., Leroy, E., Ide, S.E., Dehejia, A., Dutra, A., Pike, B., Root, H., Rubenstein, J., Boyer, R., Stenroos, E.S., Chandrasekharappa, S., Athanassiadou, A., Papapetropoulos, T., Johnson, W.G., Lazzarini, A.M., Duvoisin, R.C., Di Iorio, G., Golbe, L.I., Nussbaum, R.L., 1997. Mutation in the alpha-synuclein gene identified in families with Parkinson's disease. Science 276, 2045–2047.

Rane, N.S., Yonkovich, J.L., Hegde, R.S., 2004. Protection from cytosolic prion protein toxicity by modulation of protein translocation. EMBO J. 23, 4550–4559.

Saigoh, K., Wang, Y.L., Suh, J.G., Yamanishi, T., Sakai, Y., Kiyosawa, H., Harada, T., Ichihara, N., Wakana, S., Kikuchi, T., Wada, K., 1999. Intragenic deletion in the gene encoding ubiquitin carboxy-terminal hydrolase in gad mice. Nat. Genet. 23, 47–51.

Sandmann-Keil, D., Braak, H., Okochi, M., Haass, C., Braak, E., 1999. Alpha-synuclein immunoreactive Lewy bodies and Lewy neurites in Parkinson's disease are detectable by an advanced silver-staining technique. Acta Neuropathol. (Berl.) 98, 461–464.

Sasahara, M., Fries, J.W., Raines, E.W., Gown, A.M., Westrum, L.E., Frosch, M.P., Bonthron, D.T., Ross, R., Collins, T., 1991. PDGF B-chain in neurons of the central nervous system, posterior pituitary, and in a transgenic model. Cell 64, 217–227.

Singleton, A.B., Farrer, M., Johnson, J., Singleton, A., Hague, S., Kachergus, J., Hulihan, M., Peuralinna, T., Dutra, A., Nussbaum, R., Lincoln, S., Crawley, A., Hanson, M., Maraganore, D., Adler, C., Cookson, M.R., Muenter, M., Baptista, M., Miller, D., Blancato, J., Hardy, J., Gwinn-Hardy, K., 2003. Alpha-synuclein locus triplication causes Parkinson's disease. Science 302, 841.

Uchihara, T., Nakamura, A., Mochizuki, Y., Hayashi, M., Orimo, S., Isozaki, E., Mizutani, T., 2005. Silver stainings distinguish Lewy bodies and glial cytoplasmic inclusions: comparison between Gallyas-Braak and Campbell-Switzer methods. Acta Neuropathol. (Berl.) 110, 255–260.

Valente, E.M., Abou-Sleiman, P.M., Caputo, V., Muqit, M.M., Harvey, K., Gispert, S., Ali, Z., Del Turco, D., Bentivoglio, A.R., Healy, D.G., Albanese, A., Nussbaum, R., Gonzalez-Maldonado, R., Deller, T., Salvi, S., Cortelli, P., Gilks, W.P., Latchman, D.S., Harvey, R.J., Dallapiccola, B., Auburger, G., Wood, N.W., 2004. Hereditary early-onset Parkinson's disease caused by mutations in PINK1. Science 304, 1158–1160.

Vila, M., Przedborski, S., 2004. Genetic clues to the pathogenesis of Parkinson's disease. Nat. Med. 10 (Suppl.), S58–S62.

Von Coelln, R., Thomas, B., Savitt, J.M., Lim, K.L., Sasaki, M., Hess, E.J., Dawson, V.L., Dawson, T.M., 2004. Loss of locus coeruleus neurons and reduced startle in parkin null mice. Proc. Natl. Acad. Sci. U.S.A. 101, 10744–10749.

Wang, Y.L., Liu, W., Sun, Y.J., Kwon, J., Setsuie, R., Osaka, H., Noda, M., Aoki, S., Yoshikawa, Y., Wada, K., 2006. Overexpression of ubiquitin carboxyl-terminal hydrolase L1 arrests spermatogenesis in transgenic mice. Mol. Reprod. Develop. 73, 40–49.

Wang, Y.L., Takeda, A., Osaka, H., Hara, Y., Furuta, A., Setsuie, R., Sun, Y.J., Kwon, J., Sato, Y., Sakurai, M., Noda, M., Yoshikawa, Y., Wada, K., 2004. Accumulation of beta- and gamma-synucleins in the ubiquitin carboxyl-terminal hydrolase L1-deficient gad mouse. Brain Res. 1019, 1–9.

Watanabe, I., Vachal, E., Tomita, T., 1977. Dense core vesicles around the Lewy body in incidental Parkinson's disease: an electron microscopic study. Acta Neuropathol. (Berl.) 39, 173–175.

Wilkinson, K.D., Lee, K.M., Deshpande, S., Duerksen-Hughes, P., Boss, J.M., Pohl, J., 1989. The neuron-specific protein PGP 9.5 is a ubiquitin carboxyl-terminal hydrolase. Science 246, 670–673.

Zimprich, A., Biskup, S., Leitner, P., Lichtner, P., Farrer, M., Lincoln, S., Kachergus, J., Hulihan, M., Uitti, R.J., Calne, D.B., Stoessl, A.J., Pfeiffer, R.F., Patenge, N., Carbajal, I.C., Vieregge, P., Asmus, F., Muller-Minsk, B., Dickson, D.W., Meeting, T., Strom, T.M., Wszolek, Z.K., Gasser, T., 2004. Mutations in LRRK2 cause autosomal-dominant parkinsonism with allomorphic pathology. Neurone 44, 601–607.